Pergamon

Tetrahedron, Vol. 53, No. 41, pp. 14043-14072, 1997

0040-4020/97 $17.00 + 0.00

PII: S0040-4020(97)00909-5

The First Experimental Evidence for a Larger Medium-dependent Flexibility of Natural β-D-Nucleosides Compared to the α-D-Nucleosides

Christophe Thibaudeau, András Földesi and Jyoti Chattopadhyaya*

Department of Bioorganic Chemistry, Box 581, Biomedical Centre,
University of Uppsala, S-751 23 Uppsala, Sweden

(E-mail: jyoti@bioorgchem.uu.se. Fax: +4618554495]

Abstract: A pairwise comparison of the free-energy of the two-state N (North, *C2'-exo-C3'-endo*, $0° < P < 36°$) ⇄ S (South, *C2'-endo-C3'-exo*, $144° < P < 190°$) pseudorotational equilibrium of adenine, guanine, cytosine or thymine β-D-2',3'-dideoxynucleosides (ddNs) **2**, **4**, **5**, **7** and **9** with their α-D-counterparts **1**, **3**, **6** and **8** shows that the conformation of the pentofuranose moiety is efficiently driven towards the N-type sugars in the β-D- series and to the S-type conformation in the α-D- anomers. The extent of the free-energy of stabilization of the N-type sugars in β-D-ddNs is however 2-3 times greater than the corresponding S-type sugar stabilization in α-D-ddNs. The estimation of ΔH° contribution to the free-energy shows that the intrinsic flexibility of the sugar moiety in β-D-ddNs is 2-4 times larger than in α-D-ddNs as a result of change of either temperature or pD of the medium. This enhanced modulation of conformation by the change of temperature or pD of the solution in β-D-ddNs compared to α-D-ddNs is the result of the more efficient transmission of the anomeric effect [$n(O4') \rightarrow \sigma^*_{C1'\text{-}N}$ orbital interactions between O4' lonepair of the sugar with the σ* of C1'-N bond] to drive the sugar conformation in the former compared to the latter. An important implication of this finding is that the evolutionary forces of Nature have opted for molecules that can adopt multiple conformations owing to the unique internal flexibility as a result of interaction with various ligands.

Since β-D-nucleosides are solely chosen by Nature as the ubiquitous building blocks for the storage of information in DNA and RNA, we considered it quite important to understand whether this preference is the result of any differential modulation of internal degree of freedom of conformation of the sugar-phosphate backbone in α-D- versus β-D-nucleosides. In this work, we have chosen pairs of simple α-D- and β-D-ddNs, as models to investigate whether there is an energetic bias for the β-D- configured nucleosides over their α-D-counterparts. The reason for the choice of ddNs as models is that it is only the *N*-aglycone effect, consisting of the counteracting (i) anomeric effect (O4'-C1'-N interactions: $n(O4') \rightarrow \sigma^*_{C1'\text{-}N}$ orbital overlap) and (ii) steric effect of the nucleobase that is responsible for the drive of the sugar conformation, unlike in β-D-2'-deoxy or ribonucleosides where the preferred conformation of the sugar moiety can be explained by the complex interplay of both gauche and anomeric effects[1]. Another important reason for the choice of ddNs is that it allows us to define the conformation (8 vicinal $^3J_{HH}$) of the constituent sugar moiety more accurately than in 2'-deoxy (5 vicinal $^3J_{HH}$) or in the ribo (3 vicinal $^3J_{HH}$) series.

The following conclusions can be drawn through the pairwise comparative study of the thermodynamics of

the pD-dependent two-state N ⇄ S pseudorotational equilibrium of the pentofuranose moiety in α-D-ddNs **1**, **3**, **6** and **8** versus β-D-ddNs **2**, **4**, **7** and **9** in D_2O solution (Scheme 1): (i) The evaluation of the free-energies (ΔG°) of N⇄ S equilibrium of the pentofuranose moiety shows that the preference for S-type sugar in α-D-ddNs **1**, **3**, **6** and **8** at room temperature at any pD is much reduced compared to the preference for the N-type sugars in β-D-ddNs **2**, **4**, **7** and **9**. (ii) The conformation of the sugar moiety (ΔG°) in α-D-ddN is less readily modulated than in β-D-ddN counterpart by protonation or deprotonation of constituent nucleobase as a result of

α-D-series

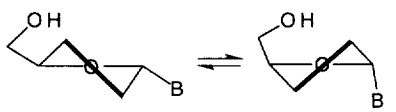

North (N) α-D-sugar ($C_{3'}$-*endo*-$C_{2'}$-*exo*) South (S) α-D-sugar ($C_{2'}$-*endo*-$C_{3'}$-*exo*)

1: α-D-ddA (B = A)
3: α-D-ddG (B = G)
6: α-D-ddC (B = C)
8: α-D-ddT (B = T)

β-D-series

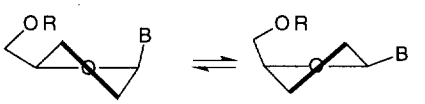

North (N) β-D-sugar ($C_{3'}$-*endo*-$C_{2'}$-*exo*) South (S) β-D-sugar ($C_{2'}$-*endo*-$C_{3'}$-*exo*)

2: β-D-ddA (B = A, R = H)
4: β-D-ddG (B = G, R = H)
5: 5'OMe-β-D-ddG (B = G, R = OMe)
7: β-D-ddC (B = C, R = H)
9: β-D-ddT (B = T, R = H)

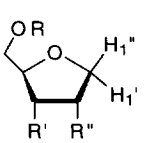

10: R = R" = H; R' = OMe
11: R = Me; R' = OMe; R" = H
12: R = R' = R" = H
13: R = R" = H; R' = OH
14: R = H; R' = R" = OH

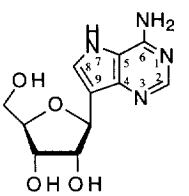

15

A = adenin-9-yl G = guanin-9-yl C = cytosin-1-yl T = thymin-1-yl

Scheme 1 : The dynamic two-state N ⇌ S sugar equilibrium in α-D-ddNs **1**, **3**, **6** and **8** versus β-D-ddNs **2**, **4**, **5**, **7** and **9** and in abasic sugars **10** and **11**. In α-D-ddNs, the aglycone B becomes more pseudoaxial as the anomeric effect becomes stronger in the S-type conformation, whereas in β-D-ddNs, this is achieved in the N-type conformation.

the change of the pD of the medium. (iii) The strength of the *N*-aglycone effect (ΔH°) of the constituent nucleobase is considerably weaker in α-D-ddNs than in β-D-ddNs. (iv) In the case of purine ddNs, it has been possible for the first time to show quantitatively that the strength of anomeric effect in the protonated adenin-9-yl in ddA or guanin-9-yl in ddG depends upon the configuration at C1', whereas they are comparable in the

neutral and the deprotonated states. (v) This means that the poorer flexibility ($\Delta G°$) of the sugar conformation in α-D-ddNs makes it less prone to respond to any change of the medium such as pH, temperature or to any ligand complexation to its own nucleobase compared to β-D-ddNs.

(A) The quantitation of the competing anomeric and gauche effects through the analysis of the thermodynamics of the two-state N ⇄ S equilibrium of the sugar conformation in nucleosides

(i) Our pD-dependent thermodynamic analysis of the N ⇄ S equilibrium of 30 interrelated analogs including abasic sugars, β-D-ddNs, β-D-2'-dNs, β-D-rNs and their 3'-phosphates, has uniquely shown[1,2] that the conformation of the sugar moiety in β-D-nucleosides is energetically ($\Delta H°$) controlled by the following stereoelectronic effects[1]: (a) The anomeric effect[1,10-12] of the nucleobase, which drives the N⇄ S equilibrium toward N-type conformations giving a pseudoaxial orientation of the aglycone, and is opposed by its counteracting steric bulk which favours its pseudoequatorial orientation. (b) The gauche effects[1,13] of [O4'-C4'-C3-O3'] and [O2'-C2'-C1'-N(Base)] fragments drive the N⇄ S equilibrium toward S-type conformers whereas the gauche effect of [O4'-C1'-C2'-O2'] drives it toward N-type sugars, and (c) the effect of [O5'-C5'-C4'-O4'] fragment is minimal.

The strength of the combined steric and stereoelectronic components of the *N*-aglycone effect is nucleobase-dependent and it increases in the following order[1]: adenine ≈ guanine, thymine, uracil, cytosine. We have recently shown[1n] that the strength of the anomeric effect ($\Delta H°$) increases (decreases) upon protonation (deprotonation) of the constituent nucleobase in β-D-2'-dNs and β-D-rNs, which has been experimentally evidenced by the sigmoidal dependence of the $\Delta G°$ of the N ⇄ S equilibrium of their pentofuranose moieties upon the pD of the solution.

(ii) In ddNs the conformation of the pentofuranose moiety is almost exclusively controlled by the strength of the substituent effect of the nucleobase[1], which drives the N ⇄ S equilibrium toward N-type sugars in the case of β-D-ddNs and toward S-type conformations in α-D-ddNs. Therefore, α-D-ddNs and β-D-ddNs constitute the systems of choice to investigate the influence of the configuration at C1' on the thermodynamics of the N ⇄ S equilibrium of their constituent sugar moieties. It has been shown that the contribution of the 5'CH_2OH effect to $\Delta H°$ of the N⇄ S equilibrium in β-D-ddNs **2**, **4**, **7** and **9** is negligible[1]. However, in order to rule out any contribution form the possible interaction between 5'CH_2OH and the nucleobase to the thermodynamics of the N ⇄ S equilibrium in β-D-ddNs, we have also determined the pD-dependent conformational preferences of the sugar moiety in 5'-OMe-β-D-ddG **5** from pD 2.0 to pD 11.9.

(B) The aromatic nature of a particular nucleobase is identical in α-D- and in β-D-ddNs

The experimentally measured aromatic ^1H chemical shifts in **1** - **9** as a function of pD have been fitted to the Henderson-Hasselbach equation (1) using a Monte Carlo algorithm[14] to give the pK_as of the nucleobases at the inflection points [see panel (A) for α-D-ddA **1**, panel (B) for β-D-ddA **2**, panel (E) for α-D-ddC **6**, panel (F) for α-D-ddC **7**, panel (I) for α-D-ddT **8** and panel (J) for β-D-ddT **9** in Fig. 3; see panels (A), (B) and (C) for α-D-ddG **3**, β-D-ddG **4** and 5'-OMe-β-D-ddG **5** in Fig. 4, respectively]. Note that these pK_a values[5] have also been further verified through Hill plots according to a well-known procedure[15]:

$$pD = pK_a + \log \frac{[A]}{[AH^+]} = pK_a + \log \frac{(1 - \alpha)}{\alpha} \quad \cdots\cdots \quad (1)$$

Our study shows that the pK_a values of adenine (3.7 in α-D-ddA **1**, 3.8 in β-D-ddA **2**), guanine (2.7 and 9.7

in α-D-ddG **3**; 2.6, 9.6 in β-D-ddG **4** and 2.5, 9.4 in 5'-OMe-β-D-ddG **5**), cytosine (4.1 in α-D-ddC **6**, 4.3 in β-D-ddC **7**) and thymine (9.7 in α-D-ddT **8**, 9.9 in β-D-ddT **9**) in each of the α-D- versus β-D-ddN pairs are virtually identical, as the differences observed in any α- / β- pair are within the accuracy of our measurements (± 0.1). This means that the aromatic character of the adenine, guanine, cytosine and thymine bases remains the same as the configuration at C1' is inverted from α- to β- in ddNs.

(C) The *N*-aglycone effect induced larger flexibility of β-D-ddNs 2, 4, 5, 7 and 9

The plots of ΔH° and ΔG° values for β-D-ddNs **2** [Table 3, panels (A) for ΔH° and (B) for ΔG^{288} in Fig. 1], **4** [Table 5, panels (A) for ΔH° and (B) for ΔG^{288} in Fig. 2], **5** [Table 6, panels (A) for ΔH° and (B) for ΔG^{288} in Fig. 2], **7** [Table 8, panels (C) for ΔH° and (D) for ΔG^{298} in Fig. 1], and **9** [Table 10, panels (E) for ΔH° and (F) for ΔG^{298} in Fig. 1] as a function of pD have the sigmoidal shape of titration curves, as found by us previously in the β-D-2'-dNs and β-D-rNs series[1n]. A Monte Carlo fitting procedure[14] of these curves to our experimental data using eq. (1) has given the ΔH°, -TΔS°and ΔG° values at the protonated (P subscript), neutral (N subscript) or deprotonated (D subscript) states of the N⇄ S equilibrium in β-D-ddNs **2, 4, 5, 7** and **9**, as well as the pK_as of the aglycones obtained from the pD values at the inflection points, which are identical (within ± 0.2) to those calculated independently from pD-dependent ^1H chemical shifts (Table 1).

(a) In each of the P, N and D states of β-D-ddNs **2, 4, 5, 7** and **9**, ΔH° is the main contribution to the drive of the N ⇄ S equilibrium to N-type sugar conformations, and it overrides the counteracting -TΔS° term.

(b) In order to investigate the hypothesis of a possible contribution of an interaction between 5'-CH_2OH moiety with the constituent nucleobase to the thermodynamics of the N ⇄ S equilibrium in the case of β-D-ddNs, we have compared the pD-dependent conformational preferences of the sugar moiety in D_2O both in β-D-ddG **4** and in its 5'-OMe counterpart, 5'-OMe-β-D-ddG **5**.

The conclusions of this comparison are as follows: (i) A perusal of ΔH° values of the N ⇄ S equilibrium in each of the P, N and D states for **4** and **5** in Table 1 clearly shows that the effect of 5'-OMe in the latter is almost identical to that of 5'OH in the former [ΔH° for (**5**) - ΔH° for (**4**) = -0.2 kJ/mol in the P state; 0.9 kJ/mol in the N state and 0.9 kJ/mol in the D state]. The strength of the 5'-OMe effect in **5** is comparable to that of 5'-OMe in 3',5'-O-dimethyltetrahydrofurfuryl alcohol [3',5'-diOMe-THFA] **11**, as obtained by subtraction of ΔH° of the N⇄ S equilibrium in **10** from that of **11**. [ΔΔH° (**11** - **10**) = 0.4 kJ/mol, Table 1]. Noteworthy is the fact that the actual preference of the sugar moiety for N-type sugars (reflected in ΔG°_N and ΔG°_D values, Table 1) is enhanced in 5'-OMe-β-D-ddG **5** compared to its 5'-OH counterpart β-D-ddG **4** in each of the neutral and deprotonated states, although ΔH°_N and ΔH°_D values are virtually identical for both compounds. This is the result of larger entropy stabilization (Table 1) of N-conformers both in the N compared to the D state in **5** compared to **4**. (ii) Our pD-dependent 1D-nOe difference experiments performed in each of the P, N and D states of β-D-ddG **4** and 5'-OMe-β-D-ddG **5** also show that guanine remains preferentially in *anti* orientation around the glycosidic torsion at all pDs for both compounds. The *syn/anti* ratios do not differ significantly for **4** and **5** (see the experimental section). Therefore, any differences observed in the drive of the sugar conformation in β-D-ddNs **2, 4, 5, 7** and **9** (*i.e*, reflected in ΔΔG° values) as the pD of the D_2O solution changes can safely be attributed to the change in the strength of the *N*-substituent effect (*i.e.* reflected in ΔΔH° values).

(c) Consistent with our previous work[1n] on β-D-2'-dNs and β-D-rNs, protonation of the nucleobase in β-D-ddA **2**, β-D-ddG **4** and β-D-ddC **7** results in the increased preference of their pentofuranose moieties for N-type

Table 1. Thermodynamics of the N ⇄ S pseudorotational equilibria of **1** - **11** with fully protonated, neutral and fully deprotonated nucleobases[a] and the corresponding pKa values.[b]

Compound	The energetics of N ⇄ S equilibrium when the nucleobase is fully protonated				pK_a [b]	The energetics of N ⇄ S equilibrium when the nucleobase is neutral				pK_a [b]	The energetics of N ⇄ S equilibrium when the nucleobase is fully deprotonated			
	ΔH°_P	ΔS°_P	$-T\Delta S^\circ_P$	ΔG°_P		ΔH°_N	ΔS°_N	$-T\Delta S^\circ_N$	ΔG°_N		ΔH°_D	ΔS°_D	$-T\Delta S^\circ_D$	ΔG°_D
α-D-ddA (**1**)	-1.7 (0.1)	-0.6 (0.5)	0.2 (0.1)	-1.5 (0.1)	-	-1.7 (0.1)	-0.6 (0.5)	0.2 (0.1)	-1.5 (0.1)	-	-	-	-	-
β-D-ddA (**2**)	9.2 (0.1)	17.5 (0.1)	-5.0 (0.1)	4.1 (0.1)	3.6	3.5 (0.1)	3.5 (0.4)	-0.9 (0.1)	2.6 (0.1)	-	-	-	-	-
α-D-ddG (**3**)	-8.7	-20.8	6.0	-2.7	2.7	-0.4 (0.2)	3.1 (0.6)	-0.9 (0.2)	-1.2 (0.1)	-	-0.4 (0.2)	3.1 (0.6)	-0.9 (0.2)	-1.2 (0.1)
β-D-ddG (**4**)	23.6	59.3	-17.1	6.7	2.5	3.4 (0.4)	1.0 (1.0)	-0.3 (0.2)	2.9 (0.1)	9.5	1.4 (0.1)	-1.7 (0.2)	0.5 (0.1)	1.8 (0.1)
5'-OMe-β-D-ddG (**5**)	23.4	58.3	-16.8	6.8	2.5	4.3 (0.5)	2.0 (1.7)	-0.6 (0.5)	3.6 (0.4)	9.7	2.3 (0.1)	-3.4 (0.2)	1.0 (0.1)	3.3 (0.1)
α-D-ddC (**6**)	-2.9 (0.2)	-4.7 (0.7)	1.4 (0.2)	-1.5 (0.1)	-	-2.9 (0.2)	-4.7 (0.7)	1.4 (0.2)	-1.5 (0.1)	-	-	-	-	-
β-D-ddC (**7**)	9.6 (0.2)	17.0 (0.4)	-4.9 (0.1)	4.6 (0.1)	4.2	6.6 (0.1)	10.4 (0.2)	-3.0 (0.1)	3.5 (0.1)	-	-	-	-	-
α-D-ddT (**8**)	-	-	-	-	-	-1.1 (0.1)	-2.0 (0.1)	0.6 (0.1)	-0.5 (0.1)	10.1	-0.5 (0.1)	-1.0 (0.1)	0.3 (0.1)	-0.2 (0.1)
β-D-ddT (**9**)	-	-	-	-	-	5.4 (0.1)	7.4 (0.1)	-2.2 (0.1)	3.2 (0.1)	9.8	3.5 (0.1)	3.7 (0.3)	-1.1 (0.1)	2.4 (0.1)
3'-OMe-THFA (**10**)	-	-	-	-	-	-4.6 (0.4)	-3.8 (1.2)	1.2 (0.3)	-3.4 (0.3)	-	-	-	-	-
3',5'-diOMe-THFA (**11**)	-	-	-	-	-	-4.2 (0.4)	-3.2 (1.2)	0.9 (0.3)	-3.3 (0.5)	-	-	-	-	-

[a] ΔH°, $-T\Delta S^\circ$ (at 288 K for **1** - **5**, at 298K for **6** - **11**) and ΔG° are in kJmol^{-1}, ΔS° in Jmol^{-1}K^{-1}. Their standard deviations (σ) are indicated in parentheses. The 'N', 'P' and 'D' subscripts denote the neutral, the protonated state and the deprotonated states, respectively. The plateaus in the P, N and D states for ΔH°, ΔS° and ΔG° values have been obtained by MonteCarlo fit of the experimental pH-dependent ΔH°, ΔG° (Fig. 1) and ΔS° (not shown) values. [b] Except for α-D-ddG (**3**), β-D-ddG (**4**) and 5'-OMe-β-D-ddG (**5**) in the acidic range, the pK_a values have been calculated through plots of experimental ΔG° of N ⇄ S pseudorotational equilibria as a function of pH and from the Hill plots of pH as a function of $\log(\Delta\Delta G^\circ_{tot} - \Delta\Delta G^\circ / \Delta\Delta G^\circ)$ (not shown). $\Delta\Delta G^\circ_{tot}$ is a total change in ΔG° values between the N and the D/P states, whereas $\Delta\Delta G^\circ$ is the change in ΔG° value at a given pH relative to the reference N state. The pK_a values were also independently determined from Hill plots based on the change in ^{1}H-NMR chemical shifts of aromatic and anomeric protons in **1** - **9** as a function of pH: for α-D-ddA (**1**) [pK_a = 3.7, 3.7 and 3.6 from δ(H8) (Panel (A) in Fig. 3), δ(H2) and δ(H1'), respectively]; for β-D-ddA (**2**) [pK_a = 3.7, 3.8 and 3.8 from δ(H8) (Panel (B) in Fig. 3), δ(H2) and δ(H1'), respectively]; for α-D-ddG (**3**) [pK_a = 2.7 and 2.6 from δ(H8) (Panel (A) in Fig. 4) and δ(H1') in the acidic range and pK_a = 9.7 from δ(H8) in the alkaline range (Panel (A) in Fig. 4)]; for β-D-ddG (**4**) [pK_a = 2.6 and 2.5 from δ(H8) (Panel (B) in Fig. 4) and δ(H1') in the acidic range and pK_a = 9.6 from δ(H8) (Panel (B) in Fig. 4) and δ(H1') in the alkaline range]; for 5'-OMe-β-D-ddG (**5**) [pK_a = 2.5 and 2.5 from δ(H8) (Panel (C) in Fig. 4) and δ(H1') in the acidic range and pK_a = 9.4 from δ(H8) (Panel (C) in Fig. 4) in the alkaline range]; for α-D-ddC (**6**) [pK_a = 4.1 from δ(H6) (Panel (E) in Fig. 3) and δ(H5)]; for β-D-ddC (**7**) [pK_a = 4.3 from δ(H6) (Panel (F) in Fig. 3) and δ(H5)]; for α-D-ddT (**8**) [pK_a = 9.7, 9.8 and 9.6 from δ(H6) (Panel (I) in Fig. 3), δ(H1') and δ(C_5-Me)]; for β-D-ddT (**9**) [pK_a = 9.8, 10.0 and 10.0 from δ(H6) (Panel (J) in Fig. 3), δ(H1') and δ(C_5-Me)]. In the case of α-D-ddG (**3**), β-D-ddG (**4**) and 5'-OMe-β-D-ddG (**5**) in the acidic pH range, the pK_as calculated from pH-dependent ^{1}H chemical shifts have been used as constraints in the determination of the plateaus in the P and N states for their respective ΔH°, ΔS° and ΔG° values during the MonteCarlo fitting procedure.

conformations [*i.e* $\Delta\Delta G°_{(P\text{-}N)}$ = 1.5 kJmol^{-1}, 3.8 kJmol^{-1} and 1.1 kJmol^{-1}, respectively] as a result of the efficient transmission of the enhancement of the strength of the *N*-aglycone effect (*i.e.* both stereoelectronic anomeric effect and the opposing steric effect) to drive the sugar conformation [*i.e* $\Delta\Delta H°_{(P\text{-}N)}$ = 5.7 kJmol^{-1}, 20.2 kJmol^{-1} and 3.0 kJmol^{-1}, respectively], whereas deprotonation of guanine in β-D-ddG **4** and of thymine in

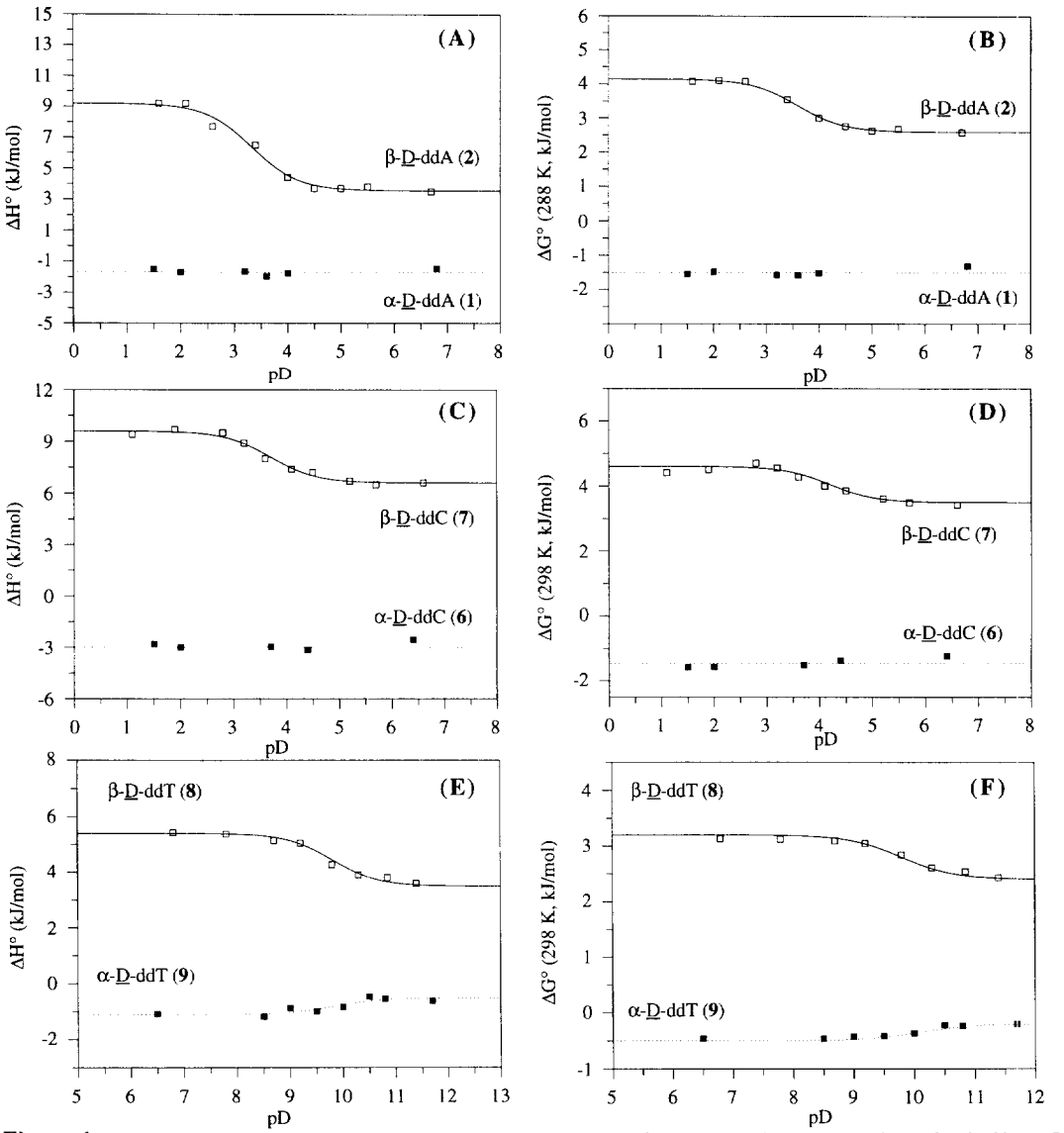

Figure 1. The plots of experimental ΔH° [Panels (A), (C) and (E)] and ΔG° values [Panels (B), (D) and (F)] for the N ⇄ S pseudorotational equilibrium of adenine, cytosine and thymine α-D- and β-D-2',3'-dideoxynucleosides. The sigmoidal curves have been fitted to our experimental data using a MonteCarlo procedure (see text and the legend of Table 1). **(A)** ΔH° values (at 6 pDs in the range 1.5 - 6.8) are pD-independent for α-D-ddA (**1**) whereas they show a sigmoidal dependence on pD for its β-counterpart β-D-ddA (**2**) (at 9 pDs in the range from 1.6 to 6.7). **(B)** ΔG^{288} values (at 6 pDs in the range 1.5 - 6.8) are pD-independent for α-D-ddA

(**1**) whereas they show a sigmoidal dependence on pD for its β-counterpart β-D-ddA (**2**) (at 9 pDs in the range from 1.6 to 6.7). **(C)** ΔH° values (at 5 pDs in the range 1.5 - 6.4) are pD-independent for α-D-ddC (**6**) whereas they show a sigmoidal dependence on pD for its β-counterpart β-D-ddC (**7**) (at 10 pDs in the range from 1.1 to 6.6). **(D)** ΔG^{298} values (at 5 pDs in the range 1.5 - 6.4) are pD-independent for α-D-ddC (**6**) whereas they show a sigmoidal dependence on pD for its β-counterpart β-D-ddC (**7**) (at 10 pDs in the range from 1.1 to 6.6). **(E)** ΔH° values both for α-D-ddT (**8**) (at 8 pDs in the range 6.5 - 11.7) and for its β-counterpart β-D-ddT (**9**) (at 8 pDs in the range 6.8 - 11.4) show a sigmoidal dependence on pD. **(F)** ΔG^{298} values both for α-D-ddT (**8**) (at 8 pDs in the range 6.5 - 11.7) and for its β-counterpart β-D-ddT (**9**) (at 8 pDs in the range 6.8 - 11.4) show a sigmoidal dependence on pD.

β-D-ddT **9** yields a reduced proportion of N-type sugars at alkaline compared to neutral pDs [$\Delta\Delta G^{\circ}_{(D\text{-}N)}$ = -1.1 kJmol^{-1} and -0.8 kJmol^{-1}, respectively] owing to the reduction of the strength of the *N*-aglycone effect [$\Delta\Delta H^{\circ}_{(D\text{-}N)}$ = -2.0 kJmol^{-1}, -1.9 kJmol^{-1}, respectively].

(d) The plots of the ^{1}H aromatic chemical shifts as a function of ΔG° of the N ⇄ S equilibrium of the constituent sugar moiety in β-D-ddNs **2**, **4**, **5**, **7** and **9** give straight lines with Pearson's correlation coefficients above 0.97 [for slopes and intercepts of the correlation plots, see the legends of panels (D), (H), (L) for **2**, **7** and **9**, respectively, in Figure 3 and panels (E) and (F) for **4** and **5**, respectively, in Fig. 4]. This shows that the forces that drive the protonation ⇄ deprotonation equilibrium in β-D-ddNs **2**, **4**, **5**, **7** and **9** are efficiently transmitted to drive the two-state N ⇄ S equilibria of their constituent sugar moieties .

(D) The poorer conformational flexibility of the α-D-ddNs 1, 3, 6 and 8

In contradistinction to what we have found for β-D-ddNs **2**, **4**, **5**, **7** and **9** (*vide supra*), the conformation of the sugar moiety in α-D-ddNs **1**, **3**, **6** and **8** appears to be rather more constrained and insensitive to the change of the pD or temperature of the solution, which is experimentally evidenced by the following:

(a) The magnitude of the *N*-aglycone effect induced modulation of the drive of the N ⇄ S equilibrium of the pentofuranose moiety, as the temperature changes (reflected in the ΔH° term) is much reduced in any of the protonated, neutral or deprotonated states of α-D-ddNs **1**, **3**, **6** and **8** compared to the corresponding β-D-counterparts **2**, **4**, **5**, **7** and **9** (see Table 1).

(b) Our 1D-nOe difference experiments in the neutral state of each of the α-/β- pairs, *i.e.* α-D-ddA **1** versus β-D-ddA **2**, in α-D-ddG **3** versus β-D-ddG **4**, in α-D-ddC **6** versus β-D-ddC **7** as well as in α-D-ddT **8** versus β-D-ddT **9** clearly show that (i) adenine, guanine, cytosine and thymine nucleobases all prefer *anti* orientation around the glycosidic torsion in all ddNs, and (ii) the extent of the preference for *anti* rotamers is almost independent upon the configuration at C1' within each α-/β- pair (see the experimental section). This therefore means that if we observe any differential modulation of the bias of the N ⇄ S equilibrium in α- compared to β-D-ddNs at any pD, this can directly be attributed to the different strength of the *N*-aglycone effect depending upon the configuration of the ddN at C1'.

(b) The preference for the population of the S-type conformations in the neutral state in α-D-ddA **1** and α-D-ddC **6** is not affected as their nucleobases become protonated [see pD-independent ΔG° values in Panels (B) and (D) of Fig. 1] compared to the β-D- counterparts. This means that although the electronic nature of the protonated and neutral nucleobases is the same both in α- and β-counterparts (*vide supra*), the change of the aromatic character from the neutral to the protonated form is not transmitted through the *N*-aglycone effect to alter the sugar conformation in the former [see the pD-independent ΔH° values in Fig. 1 for α-D-ddA **1** in Panel (A) and for α-D-ddC **6** in Panel (C)]. Similarly, upon deprotonation of guanin-9-yl in α-D-ddG **3**, the sugar conformation remains the same in the alkaline pD range as under neutral conditions compared to β-D-

ddG **4** and **5** , thereby showing the lack of transmission of the electronic character of the deprotonated guanine moiety through *N*-aglycone effect to drive its sugar conformation [see Panels (A) and (B) in Fig. 2].

(c) The only situations in which the sugar conformation of α-D-ddNs responds to the change of the pD of the solution have been found for α-D-ddG **3** in the acidic solution and for α-D-ddT **8** under alkaline conditions

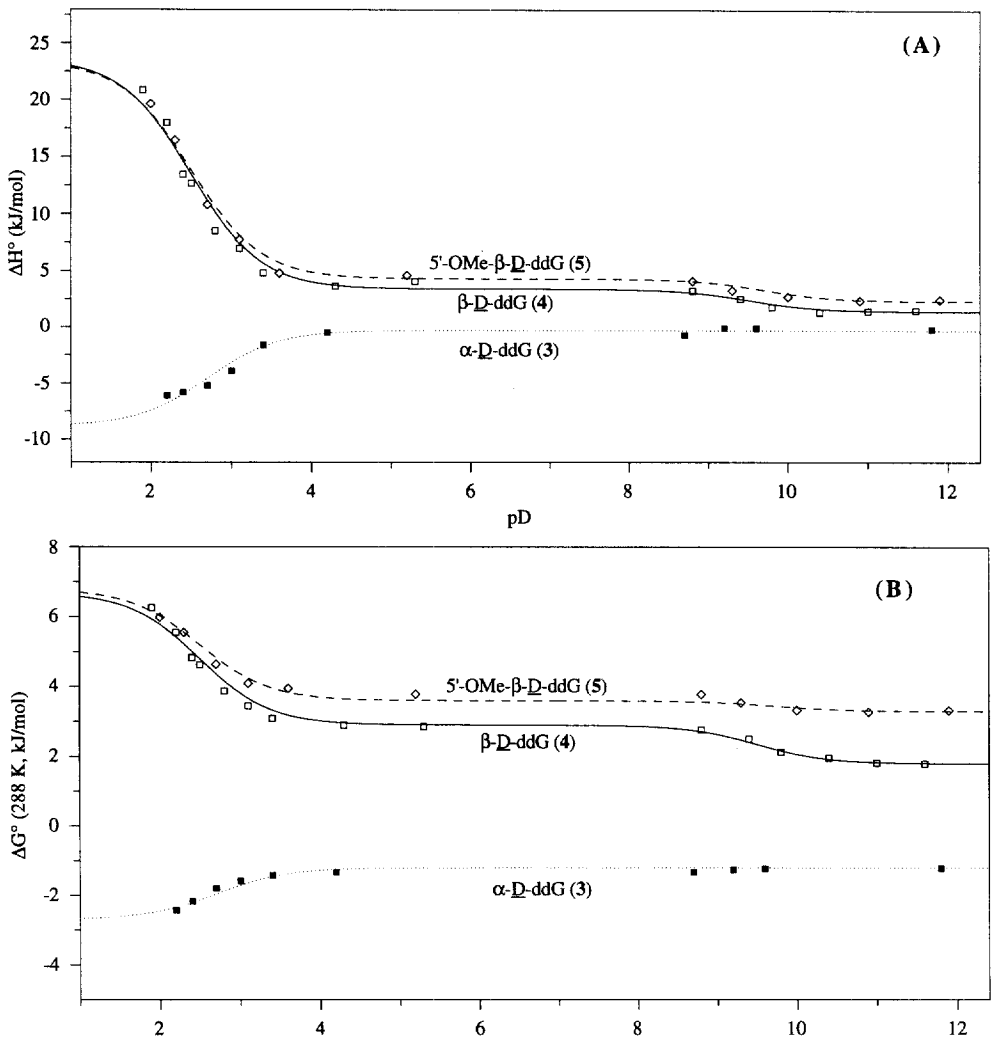

Figure 2. The plots of experimental ΔH° [Panel (A)] and ΔG° values [Panel (B)] for the N ⇄ S pseudorotational equilibrium of guanine α-D- and β-D-2',3'-dideoxynucleosides. The sigmoidal curves have been fitted to our experimental data using a MonteCarlo procedure (see text and the legend of Table 1). **(A)** ΔH° values for α-D-ddG (**3**) (at 10 pDs in the range 2.2 - 11.8), for its β-counterpart β-D-ddG (**4**) (at 15 pDs in the range 1.9 - 11.6) and for 5'-OMe-β-D-ddG (**5**) (at 11 pDs in the range 2.0 - 11.9) all show a sigmoidal dependence on pD. **(B)** ΔG^{288} values for α-D-ddG (**3**) (at 10 pDs in the range 2.2 - 11.8), for its β-counterpart β-D-ddG (**4**) (at 15 pDs in the range 1.9 - 11.6) and for 5'-OMe-β-D-ddG (**5**) (at 11 pDs in the range 2.0 - 11.9) all show a sigmoidal dependence on pD.

[$\Delta\Delta G°_{(P-N)}$ = -1.5 kJmol^{-1} for α-D-ddG **2** ; $\Delta\Delta G°_{(D-N)}$ = 0.3 kJmol^{-1} for α-D-ddT **8**], owing to the resulting enhanced [$\Delta\Delta H°_{(P-N)}$ = -8.3 kJmol^{-1}] and reduced [$\Delta\Delta H°_{(D-N)}$ = 0.6 kJmol^{-1}] *N*-substituent effect in the protonated α-D-ddG **3** and in the deprotonated α-D-ddT **8** compared to their neutral forms, respectively (see panels (E) and (F) for α-D-ddT **8** in Fig. 1 and panels (A) and (B) in Fig. 2 for α-D-ddG **3**). In these cases, the experimental pD-dependent ΔH° and ΔG° values of the N ⇄ S equilibrium could be fitted to sigmoidal curves (as described before). The pK_a value of thymine in α-D-ddT **8** determined from the pD-dependent

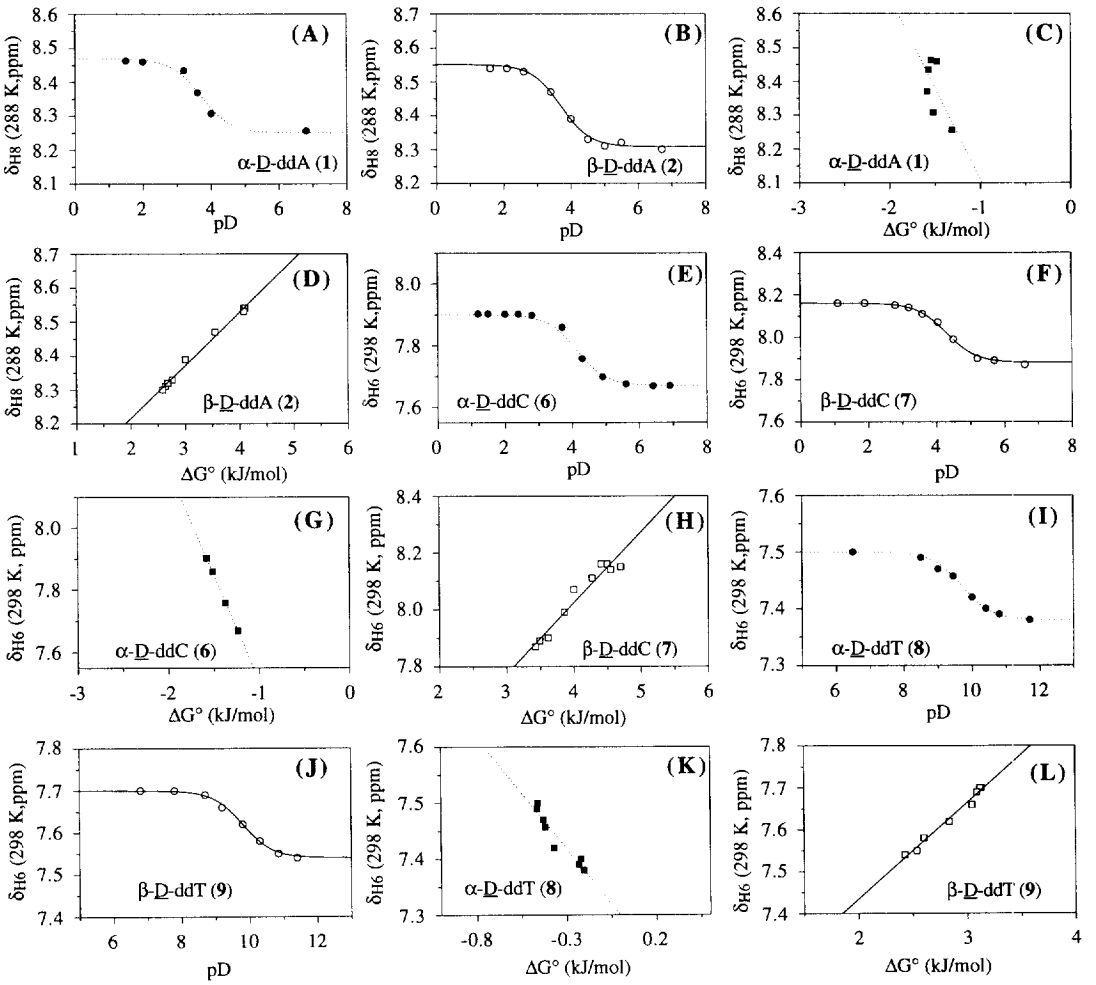

Figure 3. The plots of ^{1}H aromatic chemical shifts as a function of pD and the correlation plots of ^{1}H aromatic chemical shifts with ΔG° of the N ⇄ S equilibrium in α-D- and β-D-2',3'-ddNs. **(A)** The plot of pD-dependent H8 chemical shift (288K) for α-D-ddA (**1**), showing a sigmoidal curve which is the best iterative least-squares fit of the 6 pD-dependent experimental data. **(B)** The plot of pD-dependent H8 chemical shift (288K) for β-D-ddA (**2**), showing a sigmoidal curve which is the best iterative least-squares fit of the 9 pD-dependent experimental data. **(C)** The correlation plot of the pD-dependent H8 chemical shift (288 K) as a function of pD-dependent ΔG^{288} for the N ⇄ S equilibrium of α-D-ddA (**1**) showing a straight line, with a correlation coefficient of 0.623, a slope of

-0.53 (σ = 0.32) and an intercept of 7.58 (σ = 0.49). **(D)** The correlation plot of the pD-dependent H8 chemical shift at 288 K as a function of pD-dependent ΔG^{288} for the N$\rightleftarrows$S equilibrium of β-D-ddA (**2**) showing a straight line, with a correlation coefficient of 0.999, a slope of 0.16 (σ = 0.01) and an intercept of 7.90 (σ = 0.02). **(E)** The plot of pD-dependent H6 chemical shift (298 K) for α-D-ddC (**6**), showing a sigmoidal curve which is the best iterative least-squares fit of the 11 pD-dependent experimental data. **(F)** The plot of pD-dependent H6 chemical shift (298 K) for β-D-ddC (**7**), showing a sigmoidal curve which is the best iterative least-squares fit of the 10 pD-dependent experimental data. **(G)** The correlation plot of the pD-dependent H6 chemical shift (298 K) as a function of pD-dependent ΔG^{298} for the N$\rightleftarrows$S equilibrium of α-D-ddC (**6**) showing a straight line, with a correlation coefficient of 0.999, a slope of -0.69 (σ = 0.01) and an intercept of 6.81 (σ = 0.02). **(H)** The correlation plot of the pD-dependent H6 chemical shift (298 K) as a function of pD-dependent ΔG^{298} for the N$\rightleftarrows$S equilibrium of β-D-ddC (**7**) showing a straight line, with a correlation coefficient of 0.970, a slope of 0.25 (σ = 0.02) and an intercept of 7.03 (σ = 0.09). **(I)** The plot of pD-dependent H6 chemical shift (298 K) for α-D-ddT (**8**), showing a sigmoidal curve which is the best iterative least-squares fit of the 8 pD-dependent experimental data. **(J)** The plot of pD-dependent H6 chemical shift (298 K) for β-D-ddT (**9**), showing a sigmoidal curve which is the best iterative least-squares fit of the 8 pD-dependent experimental data. **(K)** The correlation plot of the pD-dependent H6 chemical shift (298 K) as a function of pD-dependent ΔG^{298} for the N$\rightleftarrows$S equilibrium of α-D-ddT (**7**) showing a straight line, with a correlation coefficient of 0.96, a slope of -0.39 (σ = 0.05) and an intercept of 7.30 (σ = 0.02). **(L)** The correlation plot of the pD-dependent H6 chemical shift (298 K) as a function of pD-dependent ΔG^{298} for the N$\rightleftarrows$S equilibrium of β-D-ddT (**9**) showing a straight line, with a correlation coefficient of 0.991, a slope of 0.23 (σ = 0.01) and an intercept of 6.98 (σ = 0.04).

thermodynamics of its N$\rightleftarrows$S equilibrium is almost identical (± 0.3) to that found from its pD-dependent ^{1}H chemical shifts. For α-D-ddG **3** in the acidic solution, we have fitted the sigmoidal curve to our experimental data points by constraining the value of the pK_a to that derived from ^{1}H pD-dependent chemical shifts during the MonteCarlo fit owing to the fact that pD-dependent thermodynamics of the N$\rightleftarrows$S equilibrium in this compound could not be determined at pD < 2.2 owing to its depurination (see the legend of Table 1).

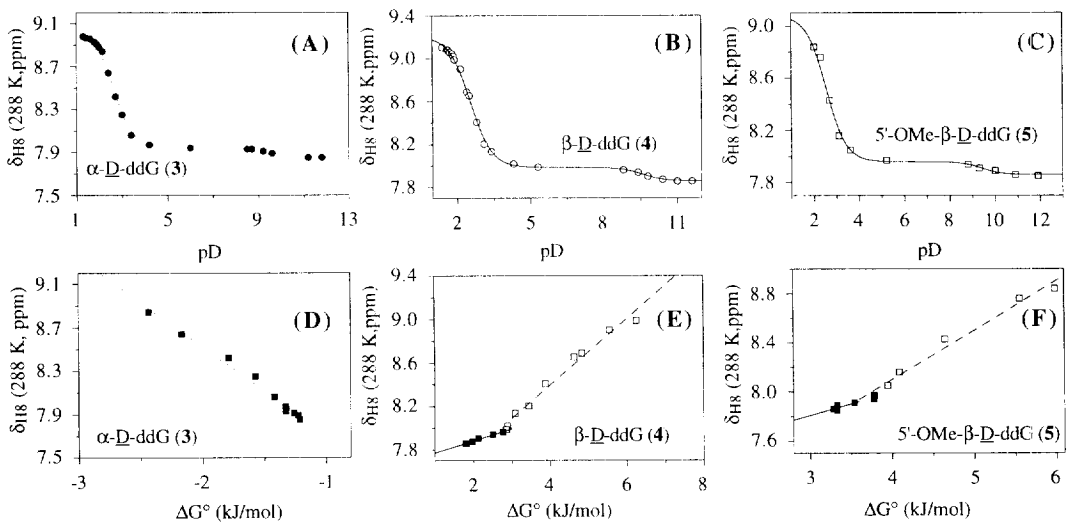

Figure 4. The plots of ^{1}H aromatic chemical shifts as a function of pD and the correlation plots of ^{1}H aromatic chemical shifts with $\Delta G°$ of the N$\rightleftarrows$S equilibrium in α-D- and β-D-2',3'-ddNs. **(A)** The plot of pD-dependent H8 chemical shift (288 K) for α-D-ddG (**3**), showing a sigmoidal curve which is the best iterative least-squares fit of the 19 pD-dependent experimental data. **(B)** The plot of pD-dependent H8 chemical shift (288 K) for β-D-ddG (**4**), showing a sigmoidal curve which is the best iterative least-squares fit of the 15 pD-dependent experimental data. **(C)** The plot of pD-dependent H8 chemical shift (288 K) for 5'-OMe-β-D-ddG (**5**), showing a sigmoidal curve which is the best iterative least-squares fit of the 19 pD-dependent experimental data. **(D)** The correlation plot of the pD-dependent H8 chemical shift (288 K) as a function of pD-dependent ΔG^{288} for the N$\rightleftarrows$S equilibrium of α-D-ddG (**3**) showing a straight line with a correlation coefficient of 0.993, a slope of -0.82 (σ = 0.06) and an intercept of 6.89 (σ = 0.03). **(E)** The correlation plots of the pD-dependent H8 chemical shift (288 K) as a function of pD-dependent ΔG^{288} for the N$\rightleftarrows$S equilibrium of β-

D-ddG (**4**) showing straight lines. The line (----) has a correlation coefficient of 0.989, a slope of 0.31 (σ = 0.02) and an intercept of 7.17 (σ = 0.07), whereas the line (—) has a correlation coefficient of 0.995, a slope of 0.12 (σ = 0.01) and an intercept of 7.65 (σ = 0.01). **(F)** The correlation plots of the pD-dependent H8 chemical shift (288 K) as a function of pD-dependent ΔG^{288} for the N ⇄ S equilibrium of 5'-OMe-β-D-ddG (**5**) showing straight lines. The line (----) has a correlation coefficient of 0.991, a slope of 0.40 (σ = 0.03) and an intercept of 6.49 (σ = 0.13), whereas the line (—) has a correlation coefficient of 0.940, a slope of 0.19 (σ = 0.03) and an intercept of 7.24 (σ = 0.12).

(d) The correlation plots of the pD-dependent ^{1}H chemical shifts as a function of the $\Delta G°$ of the N ⇄ S equilibrium in α-D-ddNs **1**, **3**, **6** and **8**, also give straight lines as in the β-counterparts (Pearson's correlation coefficients (R) > 0.96 except for α-D-ddA (**1**) (R = 0.62) because of the very small change in the experimental $\Delta G°$ values as a function of pD) [for slopes and intercepts of the correlation plots, see the legends of Panel (C) in Fig. 3 for α-D-ddA **1**, Panel (D) in Fig. 4 for α-D-ddG **3**, Panel (G) in Fig. 3 for α-D-ddC **6** and Panel (K) in Fig. 3 for α-D-ddT (**8**)]. The reduced efficiency of the transmission of the change of the strength of the *N*-aglycone effect by the pD of the solution to drive the sugar conformation for each nucleobase in α-D- compared to β-D-ddNs is also reflected in the larger slopes of these plots for the former compared to the latter (Fig. 3 and 4).

(E) The anomeric effect of *N*-aglycone on the drive of the sugar conformation is larger in purine β-D-ddNs than in α-D- counterparts in the protonated state

(i) The total N-aglycone effect in α-D- or β-D- ddNs. The total effect ($\Delta\Delta H°_1$, in columns 2, 3 and 4 of Table 2) of the *N*-aglycone in α-D-ddNs **1**, **3**, **6** and **8** compared to β-D-ddNs **2**, **4**, **5**, **7** at any pD can be quantified by simple subtraction of $\Delta H°$ of the drive of the N ⇄ S equilibrium in 1,2,3-trideoxypentofuranose **12** from $\Delta H°$ of the N ⇄ S equilibrium in a particular ddN.

(ii) The strength of the actual anomeric effect in α-D-ddA (1), β-D-ddA (2), α-D-ddG (3) and β-D-ddG (4). The anomeric effect of the nucleobase ($\Delta\Delta H°_2$, columns 5, 6 and 7 in Table 2) in a ddN can only be determined by subtracting the inherent steric effect of the *N*-aglycone from the total (*i.e.* steric + stereoelectronic) *N*-aglycone effect on the drive of N ⇄ S equilibrium. We have recently shown[1q] that the relatively most thermodynamically stabilized S-type conformer is found in the *C*-nucleoside 9-deazaadenosine **15** in which 9-deazaadenin-9-yl as the *C*-aglycone at C1' takes up the relatively most favoured pseudoequatorial orientation between pD 8.8-12.0 ($\Delta H°$ = -14.2 kJ/mol). Under alkaline pD, $\Delta H°$ for the drive of N ⇄ S pseudorotational equilibrium in **15** is almost exclusively controlled by the steric effect of the constituent *C*-aglycone, as a result of extremely reduced stereoelectronic interaction of the lone pairs of furanose-O4' with the σ^*C1'-C9(sp^2). Therefore, 9-deazaadenin-9-yl as the *C*-aglycone at C1' in **15** can be used as the best reference point for subtraction of the steric effect of the adenin-9-yl or guanin-9-yl substituent in α-D-ddA (**1**) and its β-counterpart β-D-ddA (**2**) as well as in α-D-ddG (**3**) and its β-counterpart β-D-ddG (**4**). Our results (Table 2, columns 5, 6 and 7) clearly show the enhanced strength of the anomeric effect of protonated adenine in β-D-ddA (**2**) compared to its α-counterpart α-D-ddA (**1**) and of protonated guanine in β-D-ddG (**4**) compared to its α-counterpart α-D-ddG (**3**), whereas in the neutral and deprotonated states, the strength of the anomeric effect of the nucleobase is comparable in the α-D- and β-D-series.

Table 2: The pD-dependent strength of the anomeric effect in purine α-D- and β-D-ddNs

Compound	$\Delta\Delta H^\circ_1$ = Effect of the *N*-aglycone[a]			$\Delta\Delta H^\circ_2$ = Anomeric Effect of the *N*-aglycone[b]		
	Protonated nucleobase	Neutral nucleobase	Deprotonated nucleobase	Protonated nucleobase	Neutral nucleobase	Deprotonated nucleobase
α-D-ddA (**1**)	-2.1	-2.1	-	-16.7	-16.7	-
β-D-ddA (**2**)	8.8	3.1	-	23.4	17.7	
α-D-ddG (**3**)	-9.1	-0.8	-0.8	-23.7	-15.4	-15.4
β-D-ddG (**4**)	23.2	3.0	1.0	37.8	17.6	15.6

[a] $\Delta\Delta H^\circ_1$ = the total effect of the *N*-aglycone on the N ⇄ S equilibrium of **1** - **4** has been calculated by subtracting the gauche effect of 5'-CH_2OH group (reflected in the ΔH° value of the N ⇄ S equilibrium for **12**) from the experimental ΔH° values for **1** - **4** (see ref. 1a)

[b] $\Delta\Delta H^\circ_2$ = the anomeric effect of adenine in α-D-ddA **1** and β-D-ddA **3** and of guanine in α-D-ddG and β-D-ddG is given by the equation: $\Delta\Delta H^\circ_2 = \Delta\Delta H^\circ_1$ - SE (Base), where SE (Base) denotes steric effect of adenine (or guanine) on the N ⇄ S equilibrium of **1** - **4**. For β-D-ddA and β-D-ddG, SE (Base) = ΔH° of (**15**) - ΔH° of (**14**) = -14.2 -0.4 = -14.6 kJ/mol (see ref. 1q). For α-D-ddA and α-D-ddG, we have assumed in first approximation that the steric effect of the adenine and guanine base has the same strength as in the β-counterparts, but is of opposite sign due to the opposite configuration at C1', driving the N ⇄ S equilibrium to N-type conformations. Therefore SE (Base) = - [ΔH° of (**15**) - ΔH° of (**14**)] = -[-14.2 -0.4] = 14.6 kJ/mol. ΔH° of **15** has been taken from ref. 1q.

Conclusions

We herein have shown unambiguously that more flexible β-D-nucleosides are chosen by evolutionery forces over the α-D-nucleosides. The basic mechanisms of the flexibility differences between α-D- and β-D-nucleosides are as follows:

(i) The aromatic nature of the nucleobase remains the same as one changes the configuration at C1' from α- in α-D-ddNs **1**, **3**, **6** and **8** to β- in β-D-ddNs **2**, **4**, **5**, **7** and **9** as experimentally evidenced by their identical pK_a values.

(ii) The correlation plots of aromatic ^1H chemical shifts of the constituent nucleobase versus ΔG° of the two-state N ⇄ N equilibrium show straight lines both in the case of α-D-ddNs **1**, **3**, **6** and **8** and of their β-D-counterparts **2**, **4**, **5**, **7** and **9**. However, the slopes of the plots for the former are much larger compared to those for the latter, which means that the efficiency (ΔG°) of the anomeric effect induced modulation of the drive of the N ⇄ S equilibrium by the pD of the solution is much reduced in the former compared to the latter.

(iii) The efficiency of the transmission of the effect that drives the protonation ⇄ deprotonation equilibrium of a particular nucleobase to drive the conformation of the constituent pentofuranose moiety through the pD-dependent *N*-aglycone effect is greatly reduced in α-D-ddNs **1**, **3**, **6** and **8** compared to the situation in β-D-counterparts **2, 4**, **5**, **7** and **9**. This implies that the internal flexibility of the sugar conformation is significantly restricted in α-D-ddNs compared to β-D-ddNs. This also means that the sugar moiety in β-D-ddNs will be much more predisposed to respond to the change of the environment (*i.e.* change of the pH of the solution, metallation or interaction of the nucleobase with any other ligand) than that in α-D-ddNs **1**, **3**, **6** and **8**.

Our results therefore suggest that it is the inherent flexibility of the conformation of the sugar moieties that makes β-D-nucleosides the universal building blocks for the storage of the genetic information in Nature as they appear to be more flexible, and, hence, can afford to be more promiscuous in adopting necessary

conformation as a response to the immediate environment than their α-D-counterparts.

Experimental Section

(A) Chemical syntheses. α-D-2',3'-dideoxyadenosine **1**, α-D-2',3'-dideoxyguanosine **3** and α-D-2',3-dideoxythymidine **8** were prepared in a stereocontrolled manner from the respective α-D-arabinonucleoside derivatives[17] obtained via trimethylsilyl trifluoromethanesulfonate catalysed condensation[18] of persilylated N^6-benzoyladenine[19], N^2-acetyl-O^6-diphenylcarbamoylguanine[17b] and thymine, respectively, with 1-O-acetyl-2,3,5-tri-O-(p-toluoyl)-α,β-D-arabinofuranose[20] in dry 1,2-dichloroethane. After selective removal of the p-toluoyl groups from the sugar hydroxyl functions[20b], the base protected α-D-arabinonucleosides were converted first into their 3',5'-O-(1,1,3,3-O-tetraisopropyldisiloxan-1,3-diyl)-2'-O-phenoxythiocarbonyl (PTC)[20,21] derivatives for the reduction of the C-2' center under free radical condition[21] with tri-n-butyltin hydride in the presence of 2,2'-azobis(2-methylpropionitrile) (AIBN). The α-D-2'-deoxynucleosides obtained upon removal of the silyl protection with 1M tetra-n-butylammonium fluoride in dry THF were protected as 5'-O-(p-toluoyl)-3'-O-PTC derivatives. Their free radical deoxygenation[21] and subsequent treatment with methanolic ammonia afforded compounds **1**, **3** and **8**. α-D-2',3'-dideoxycytidine **6** was prepared upon condensation of silylated N^4-benzoylcytosine[19] and 1-O-methyl-5-O-(p-toluoyl)-α,β-D-2,3-dideoxy-ribofuranose (obtained by deoxygenation of 1-O-methyl-5-O-(p-toluoyl)-3-O-PTC-α,β-D-2-deoxyribose) in dry acetonitrile[22] with trimethylsilyl triflate as Lewis acid[23] catalyst. The anomers formed were separated by short column chromatography and the α-anomer was deprotected to compound **6** by methanolic ammonia. β-D-2',3'-dideoxyguanosine **4** was obtained *via* the free radical reduction of 5'-O-(p-toluoyl)-3'-O-PTC-N^2-acetyl-O^6-diphenylcarbamoyl-2'-β-D-deoxyguanosine[21,24] followed by treatment with methanolic ammonia. 5'-O-Methyl-β-D-2',3'-dideoxyguanosine **5** was synthesised from 5'-O-methyl-2',3'-O-bis-(p-toluoyl)-N^2-acetyl-O^6-diphenylcarbamoyl-β-D-guanosine obtained upon condensation of silylated N^2-acetyl-O^6-diphenylcarbamoylguanine and 1-O-acelyl-2,3-O-bis-(p-toluoyl)-5-O-methyl-α,β-D-ribofuranose. Removal of p-toluoyl groups according to a literature procedure[24b] and protection of the *cis* 2',3'-diol with a 2'-O-(*tert*-butyldimethylsilyl)-3'-O-phenoxythiocarbonyl combination allowed the deoxygenation with tri-n-butyltin hydride and AIBN to afford 2'-O-TBDMS-3'-deoxyguanosine derivative. This was converted to 2'-O-PTC-3'-deoxy derivative, deoxygenated and deprotected by methanolic ammonia. Compound **10** was prepared *via* methylation of 5-O-monomethoxytrityl-1,2-dideoxy-D-ribofuranose[1a] with methyl iodide in the presence of NaH in dry DMF[25] followed by removal of the 5-O-protecting group according to our literature procedure[1a]. Methylation of compound **10** as above afforded compound **11**.

(B) ^{1}H-NMR spectroscopy. ^{1}H-NMR spectra have been recorded throughout the 278 K - 358 K range in 5 K or 10 K intervals in D_2O solution at various pDs in the 1.1 - 11.6 range using 500 MHz or 600 MHz Bruker DRX spectrometers (see Tables 12 - 20). At each pD, $^3J_{HH}$ extracted from ^{1}H-NMR spectra have been simulated and/or iterated with the DAISY program[16]. The FIDs have been recorded using 32 K points and the spectra have been zero-filled to 64 K. The configurations at C1' of α-D-ddNs **1**, **3**, **6** and **8** have been verified using 1D-^{1}H-nOe difference spectroscopy.

The relative populations of *syn* and *anti* rotamers in the *syn* ⇄ *anti* equilibrium around the glycosidic torsion in α-D-ddNs **1**, **3**, **6** and **8** and in their β-counterparts **2**, **4**, **5**, **7** and **9** have been determined by 1D ^{1}H nOe difference spectroscopy (at 288 K or at 298 K in D_2O solution) using the method described elsewhere by

Rosemeyer et. al.[26]. For each compound, we have performed two experiments: in the first one, saturation of an aromatic proton (H8 for adenine and guanine, H6 for cytosine and thymine base) yielded an nOe at H1' ($nOe_{H1'}$), whereas in the second experiment, saturation of H1' gave an nOe at H8 (or H6) (denoted (nOe_{H6} or nOe_{H8}). The average nOe value (nOe_{av}) obtained from these two experiments gives an estimate of the population of *syn* rotamers (*% syn*) around the glysosidic torsion using the equation: *% syn* = nOe_{av} / 0.107. The results are as follows: (a) For α-D-ddA **1** (at 298 K, pD = 7.3), $nOe_{H1'}$ = 2.3 %, nOe_{H8} = 1.9 %, nOe_{av} = 2.1 % and *% syn* = 20 % ; (b) For β-D-ddA **2** (at 298 K, pD = 7.0), $nOe_{H1'}$ = 2.3 %, nOe_{H8} = 2.4 , nOe_{av} = 2.4 % and *% syn* = 22 % ; (c) For α-D-ddG 3 (pD = 7.5), $nOe_{H1'}$ = 1.5 %, nOe_{H8} = 2.1, nOe_{av} = 1.8 % and *% syn* = 17 % (at 298 K) and $nOe_{H1'}$ = 1.8 %, nOe_{H8} = 1.8, nOe_{av} = 1.8 % and *% syn* = 17 % (at 288 K); (d) For β-D-ddG **4** (at 288 K), $nOe_{H1'}$ = 1.4 %, nOe_{H8} = 1.5, nOe_{av} = 1.5 % and *% syn* = 14 % (at pD = 2.1); $nOe_{H1'}$ = 1.9 %, nOe_{H8} = 2.4, nOe_{av} = 2.2 % and *% syn* = 21 % (at pD = 7.4) and $nOe_{H1'}$ = 2.8 %, nOe_{H8} = 2.8, nOe_{av} = 2.8 % and *% syn* = 26 % (at pD = 11.5); (e) For 5'-OMe-β-D-ddG **5** (at 288 K), $nOe_{H1'}$ = nOe_{av} = 1.6 % and *% syn* = 15 % (at pD = 2.1); $nOe_{H1'}$ = 1.7 %, nOe_{H8} = 1.4, nOe_{av} = 1.6 % and *% syn* = 21 % (at pD = 6.6) and $nOe_{H1'}$ = 1.3 %, nOe_{H8} = 1.3, nOe_{av} = 1.3 % and *% syn* = 12 % (at pD = 11.7); (f) For α-D-ddC **6** (at 298 K, pD = 7.1), $nOe_{H1'}$ = nOe_{av} = 2.4 % and *% syn* = 22 % ; (g) For β-D-ddC **7** (at 298K, pD = 7.0), $nOe_{H1'}$ = nOe_{av} = 1.5 % and *% syn* = 14 % ; (h) For α-D-ddT **8** (at 298 K, pD = 7.2), $nOe_{H1'}$ = 3.7 %, nOe_{H6} = 3.2 %, nOe_{av} = 3.5 % and *% syn* = 33 % ; (i) For β-D-ddT **9** (at 298 K, pD = 7.0), $nOe_{H1'}$ = 2.1 %, nOe_{H6} = 2.0 %, nOe_{av} = 2.1 % and *% syn* = 20 %.

(C) Determination of the energetics of the pseudorotational equilibrium in nucleos(t)ides. The thermodynamics of the N ⇄ S equilibrium in 1 - **9** have been determined at each pD using our standard procedure[1]: The iterated or simulated $^3J_{HH}$ have been interpretated in terms of two-state N ⇄ S equilibrium[3] with the program PSEUROT[9], as they are time-average values of the $^3J_{HH}$ of the individual conformers. Five parameters are needed to describe the actual state of the N ⇄ S equilibrium: The phase angles and puckering amplitudes of the N [P_N, $\Psi_m(N)$] and S [P_S, $\Psi_m(S)$] pseudorotamers and the mole fraction of one of them (x_N or x_S). PSEUROT calculates the best fit of these five parameters to the experimental $^3J_{HH}$. The input of a PSEUROT calculation consists of sets of (i) experimental $^3J_{HH}$, (ii) substituent electronegativities[9], and (iii) starting values for P_N, P_S, $\Psi_m(N)$ and $\Psi_m(S)$ as well as x_S at each temperature. The quality of the fit is reflected in the rms of the analysis and the maximal difference (ΔJ_{max}) between $^3J_{HH}$ back-calculated by PSEUROT (using the optimized P_N, P_S, $\Psi_m(N)$ and $\Psi_m(S)$) and the experimental $^3J_{HH}$.

(a) Examination of the conformational hyperspace that is accessible to the N and S pseudorotamers. The PSEUROT calculations have been performed in either one or two ways: (i) When there is a clear preference of the sugar for either N- or S-type conformations, we have constrained the geometry of the minor conformer. (ii) We have also performed another series of calculations in which $\Psi_m(N)$ and $\Psi_m(S)$ have been fixed at an identical value. The detailed results of the PSEUROT analyses are given in Tables 3 - 11 for **1** - **9**.

For **10** and **11**, we have first constrained the phase angle of the minor N conformer in the range -40° < P_N < 40° in 10° steps with $\Psi_m(N)$ set to 28°, 29°, 30°, 31° and 32°, which resulted in 136° < P_S < 146° and 29° < $\Psi_m(S)$ < 32° for **10** [ΔJ_{max} = 0.6 Hz and r.m.s. < 0.5 Hz] and in 132° < P_S < 145° and 29° < $\Psi_m(S)$ < 32° for **11** [ΔJ_{max} = 0.6 Hz and r.m.s. < 0.4 Hz]. Alternatively, $\Psi_m(N)$ and $\Psi_m(S)$ have been constrained to the same value in the range 29° - 32° in 1° steps which resulted in -30° < P_N < 7° and 136° < P_S < 145° for **10** and in -26° < P_N < -10° and 135° < P_S < 143° for **11**. The results of the pseudorotational analyses for **12** - **14** have been reported earlier[1a] as well as for **15**[1q].

Table 3. Pseudorotational analyses of temperature-dependent $^3J_{HH}$ (from 278 to 358 K)[a] at six pDs (1.5-6.8) and determination of the pD-dependent thermodynamics of the two-state N ⇄ S equilibrium in α-D-ddA (**1**).

		Ψ_m constrained analyses in PSEUROT [b, c]		Slopes and intercepts of various van't Hoff plots from $\ln(x_S/x_N)$ vs 1000/T [e]		Thermodynamics of N ⇄ S equilibrium from van't Hoff plots [e, f]			Thermodynamics of N ⇄ S equilibrium from the average populations [g]
pD	Total number of PSEUROT analyses [d]	P_N	P_S	average slopes (σ)	average intercepts (σ)	$\Delta H°$ (σ)	$-T\Delta S°$ (σ)	$\Delta G^{288} = \Delta H° - T\Delta S°$	$\Delta G^{288} = -0.288 * R\ln_{av}(x_S/x_N)$
1.5	2892	-23° - 9°	124° - 144°	0.18 (0.14)	0.01 (0.48)	-1.5 (1.1)	0.0 (1.1)	-1.5 (1.6)	-1.5 (0.2)
2.0	2552	-24° - 8°	123° - 142°	0.20 (0.14)	-0.06 (0.49)	-1.7 (1.2)	0.2 (1.2)	-1.5 (1.7)	-1.5 (0.2)
3.2	2377	-28° - 6°	122° - 141°	0.20 (0.09)	-0.03 (0.31)	-1.7 (0.8)	0.1 (0.7)	-1.6 (1.1)	-1.6 (0.2)
3.6	2842	-29° - 4°	122° - 141°	0.24 (0.09)	-0.16 (0.31)	-2.0 (0.8)	0.4 (0.7)	-1.6 (1.1)	-1.6 (0.2)
4.0	3318	-29° - 3°	122° - 140°	0.21 (0.06)	-0.11 (0.22)	-1.8 (0.5)	0.3 (0.5)	-1.5 (0.7)	-1.5 (0.2)
6.8	1117	-27° - 3°	122° - 142°	0.18 (0.05)	-0.08 (0.19)	-1.5 (0.4)	0.2 (0.4)	-1.3 (0.6)	-1.3 (0.2)

[a] $^3J_{HH}$ at each of the six pDs at two extreme temperatures are given in Table 12. [b] Assuming Ψ_m (N) = Ψ_m (S), we have kept Ψ_m (N) and Ψ_m (S) fixed to identical values in the range from 32° to 40° at each pD and surveyed the conformational hyperspace in 1° steps during several PSEUROT optimizations which resulted in different populations of N and S conformers with their distinctive P_N and P_S. [c] The error estimates of the PSEUROT analyses have been assessed in terms of ΔJ_{max} and r.m.s., both of which are reflecting the difference between $^3J_{calc}$ and $^3J_{exp}$ coupling constants. The number of successful PSEUROT analyses in column 2 are designated to those which were within the constrained values (see experimental section) as well as having ΔJ_{max} and r.m.s. values smaller than 1.3 Hz and 0.8 Hz. [d] For each of these PSEUROT[9] calculations the coupling constants were 1000 times randomized which resulted in different populations of N and S conformers with their distinctive P_N and P_S (see experimental section). [e] The populations of N and S pseudorotamers obtained through each of the above PSEUROT calculations at different temperatures, shown in column 2, are the basis for the identical number of van't Hoff plots, which in turn were used to calculate the average slopes and intercepts. [f] The average of the slopes and the intercepts derived from all van't Hoff plots at a particular pD given in columns 5 and 6 were finally used to calculate the average $\Delta H°$, $-T\Delta S°$ (at 288 K) and subsequently ΔG^{288} (kJ/mol^{-1}) of N ⇄ S equilibria of **1**. [g] ΔG^{288} calculated directly from the average logarithm $\ln_{av}(x_S/(1-x_S))$, by using the Gibbs equation $\Delta G^T = -(RT/1000)\ln_{av}(x_S/(1-x_S))$ with $1-x_S = x_N$, R is the gas constant and T is the temperature (in K). The standard deviations are in parentheses.

Table 4. Pseudorotational analyses of temperature-dependent $^3J_{HH}$ (from 278 to 358 K)[a] at nine different pDs (1.6-6.7), and determination of pD-dependent thermodynamics of the two-state N ⇄ S equilibrium for β-D-ddA (**2**).

	Total number of PSEUROT analysis [e]	Ψ_m constrained analyses in PSEUROT [b, c]		P_S and Ψ_m(S) constrained analyses in PSEUROT [c, d]		Slopes and intercepts of various van't Hoff plots from $\ln(x_S/x_N)$ vs 1000/T [f]		Thermodynamics of N ⇄ S equilibrium from van't Hoff plots [f, g]			Thermodynamics of N ⇄ S equilibrium from the average populations [h]
pD		P_N	P_S	P_N	Ψ_m(N)	average slopes (σ)	average intercepts (σ)	ΔH° (σ)	-TΔS° (σ)	ΔG^{288}= ΔH°-TΔS°	ΔG^{288} = -0.298*R$\ln_{av}$ ($x_S/(x_N)$)
1.6	7334	-4° - 8°	121° - 161°	0° - 11°	29° - 33°	-1.1 (0.4)	2.1 (1.5)	9.2 (3.7)	-5.0 (3.7)	4.2 (5.2)	4.1 (0.3)
2.1	6619	-2° - 8°	120° - 156°	0° - 10°	29° - 33°	-1.1 (0.3)	2.1 (1.2)	9.2 (2.8)	-5.0 (2.8)	4.2 (4.0)	4.1 (0.3)
2.6	8292	-6° - 8°	120° - 159°	0° - 11°	29° - 33°	-0.9 (0.2)	1.5 (0.8)	7.7 (2.0)	-3.6 (1.9)	4.1 (2.7)	4.1 (0.4)
3.4	6304	-8° - 7°	120° - 156°	0° - 12°	29° - 33°	-0.8 (0.1)	1.2 (0.4)	6.5 (1.1)	-3.0 (1.0)	3.5 (1.5)	3.5 (0.4)
4.0	6599	-9° - 9°	120° - 155°	0° - 12°	29° - 33°	-0.5 (0.1)	0.6 (0.4)	4.4 (1.1)	-1.4 (1.0)	3.0 (1.5)	3.0 (0.4)
4.5	6525	-11° - 8°	120° - 156°	2° - 13°	29° - 33°	-0.4 (0.1)	0.4 (0.3)	3.7 (0.7)	-0.9 (0.7)	2.8 (1.0)	2.8 (0.4)
5.0	4542	-11° - 9°	120° - 155°	2° - 13°	29° - 33°	-0.4 (0.1)	0.4 (0.3)	3.7 (0.7)	-1.0 (0.7)	2.7 (1.0)	2.6 (0.4)
5.5	4969	-11° - 8°	120° - 154°	3° - 13°	29° - 33°	-0.5 (0.1)	0.5 (0.2)	3.8 (0.6)	-1.2 (0.6)	2.6 (0.8)	2.7 (0.4)
6.7	4970	-11° - 8°	120° - 156°	2° - 12°	29° - 33°	-0.4 (0.1)	0.4 (0.3)	3.5 (0.6)	-0.9 (0.6)	2.6 (0.8)	2.6 (0.4)

[a] $^3J_{HH}$ at each of nine pDs at 278 and 358 K are given in Table 13. [b] Assuming Ψ_m (N) = Ψ_m (S), we have kept Ψ_m (N) and Ψ_m (S) fixed to identical values in the range from 29° to 33° for pD = 1.6, from 30° to 32° for pD = 2.1, from 30° to 34° for pD = 2.6, from 30° to 35° for pD = 3.4, from 30° to 36° for pD = 4.0 and from 29° to 36° for pD = 4.5 to 6.7 and surveyed the conformational hyperspace in 1° steps during several PSEUROT optimizations which resulted in different populations of N and S conformers with their distinctive P_N and P_S. [c] The error estimates of the PSEUROT analyses have been assessed in terms of ΔJ_{max} and r.m.s., both of which are reflecting the difference between $^3J_{calc}$ and $^3J_{exp}$ coupling constants. The number of successful PSEUROT analyses in column 2 are designated to those which were within the constrained values (see experimental section) as well as having a ΔJ_{max} and r.m.s. values smaller than 1.2 Hz and 0.8 Hz. [d] P_S of the minor S-type conformers were fixed at $160° \leq P_S \leq 180°$ in 10° steps with Ψ_m (S) being simultaneously fixed at 30° and 32° for pD = 1.6 and 2.1, at 30°, 32° and 34° for pD = 2.6 and above 4.0 and at 30°and 35° for pD = 3.4 and 4.0 during several PSEUROT optimizations which resulted in different populations of N and S conformers with their distinctive P_N and P_S. [e] For each of these PSEUROT[9] calculations the coupling constants were 1000 times randomized which resulted in different populations of N and S conformers with their distinctive P_N and P_S (see experimental section). [f] The populations of N and S pseudorotamers obtained through each of the above PSEUROT calculations at different temperatures, shown in column 2, are the basis for the identical number of van't Hoff plots, which in turn were used to calculate the average slope and intercept. [g] The average of the slopes and the intercepts derived from all van' t Hoff plots at a particular pD given in the columns 7 and 8 were finally used to calculate the average ΔH°, -TΔS° (at 288 K) and subsequently ΔG^{288} (kJ/mol^{-1}) of N ⇄ S equilibria of **2**. [h] ΔG^{288} calculated directly from the average logarithm $\ln_{av}$ (x_S/ (1- x_S)), by using the Gibbs equation ΔG^T = -(RT/1000)$\ln_{av}$ (x_S/ (1- x_S)) with 1- x_S =x_N , R is the gas constant and T is the temperature. The standard deviations are in parentheses.

Table 5. Pseudorotational analyses of temperature-dependent $^3J_{HH}$ (from 278 to 358 K)[a] at 10 pDs (2.2 - 11.8) and determination of the pD-dependent thermodynamics of the two-state N ⇄ S equilibrium in α-D-ddG (**3**).

		Ψ_m constrained analyses in PSEUROT [b, c]		**Slopes and intercepts of various van't Hoff plots from $\ln(x_S/x_N)$ vs 1000/T** [e]		**Thermodynamics of N ⇄ S equilibrium from van't Hoff plots** [e, f]			**Thermodynamics of N ⇄ S equilibrium from the average populations** [g]
pD	Total number of PSEUROT analyses [d]	P_N	P_S	average slopes (σ)	average intercepts (σ)	ΔH° (σ)	-TΔS° (σ)	ΔG^{288} = ΔH°-TΔS°	ΔG^{288} = -0.288*R$\ln_{av}$ (x_S/x_N)
2.2	4315	-29° - 0°	129° - 141°	0.73 (0.10)	-1.51 (0.36)	-6.1 (0.9)	3.6 (0.9)	-2.5 (1.2)	-2.4 (0.1)
2.4	4789	-30° - -1°	128° - 141°	0.70 (0.12)	-1.53 (0.43)	-5.8 (1.0)	3.7 (1.0)	-2.1 (1.4)	-2.2 (0.1)
2.7	2821	-26° - 2°	126° - 140°	0.62 (0.09)	-1.41 (0.33)	-5.2 (0.8)	3.3 (0.8)	-1.9 (1.1)	-1.8 (0.1)
3.0	6056	-27° - 1°	125° - 139°	0.47 (0.11)	-0.96 (0.39)	-3.9 (0.9)	2.3 (0.9)	-1.6 (1.3)	-1.6 (0.1)
3.4	5435	-26° - 1°	123° - 137°	0.19 (0.08)	-0.05 (0.26)	-1.6 (0.6)	0.1 (0.6)	-1.5 (0.9)	-1.4 (0.1)
4.2	5513	-24° - 3°	122° - 136°	0.06 (0.06)	0.35 (0.20)	-0.5 (0.5)	-0.8 (0.5)	-1.3 (0.7)	-1.3 (0.1)
8.7	6420	-26° - 2°	122° - 136°	0.08 (0.03)	0.27 (0.12)	-0.7 (0.3)	-0.7 (0.3)	-1.4 (0.4)	-1.3 (0.1)
9.2	6370	-23° - 3°	122° - 136°	0.02 (0.03)	0.47 (0.12)	-0.1 (0.3)	-1.1 (0.3)	-1.2 (0.4)	-1.3 (0.1)
9.6	6430	-26° - 1°	122° - 136°	0.01 (0.04)	0.47 (0.12)	-0.1 (0.3)	-1.1 (0.3)	-1.2 (0.4)	-1.2 (0.1)
11.8	6634	-25° - 1°	122° - 136°	0.02 (0.03)	0.41 (0.13)	-0.2 (0.3)	-1.0 (0.3)	-1.2 (0.4)	-1.2 (0.1)

[a] $^3J_{HH}$ at each of the ten pDs at two extreme temperatures are given in Table 14. [b] Assuming $\Psi_m(N) = \Psi_m(S)$, we have kept $\Psi_m(N)$ and $\Psi_m(S)$ fixed to identical values in the range from 33° to 39° at each pD and surveyed the conformational hyperspace in 1° steps during several PSEUROT optimizations which resulted in different populations of N and S conformers with their distinctive P_N and P_S. [c] The error estimates of the PSEUROT analyses have been assessed in terms of ΔJ_{max} and r.m.s., both of which are reflecting the difference between $^3J_{calc}$ and $^3J_{exp}$ coupling constants. The number of successful PSEUROT analyses in column 2 are designated to those which were within the constrained values (see experimental section) as well as having a ΔJ_{max} and r.m.s. values smaller than 1.3 Hz and 0.8 Hz. [d] For each of these PSEUROT[9] calculations the coupling constants were 1000 times randomized which resulted in different populations of N and S conformers with their respective P_N and P_S (see experimental section). [e] The populations of N and S pseudorotamers obtained through each of the above PSEUROT calculations at different temperatures, shown in column 2, are the basis for the identical number of van't Hoff plots, which in turn were used to calculate the average slopes and intercepts. [f] The average of the slopes and the intercepts derived from all van't Hoff plots at a particular pD given in the columns 5 and 6 were finally used to calculate the average ΔH°, -TΔS° (at 288 K) and subsequently ΔG^{288} (kJ/mol^{-1}) of N ⇄ S equilibria of **3**. [g] ΔG^{288} calculated directly from the average logarithm $\ln_{av}$ (x_S/ (1- x_S)), by using the Gibbs equation $\Delta G^T = -(RT/1000)\ln_{av}$ (x_S/ (1- x_S)) with 1- x_S = x_N, R is the gas constant and T is the temperature. The standard deviations are in parentheses.

Table 6. Pseudorotational analyses of temperature-dependent $^3J_{HH}$ (from 278 to 358 K)[a] at fifteen different pDs (1.9-11.6), and determination of pD-dependent thermodynamics of the two state N ⇄ S equilibrium for β-D-ddG (**4**).

	Total number of	Ψ_m constrained analyses in PSEUROT [b, c]		P_S and Ψ_m(S) constrained analyses in PSEUROT [c, d]		Slopes and intercepts of various van't Hoff plots from $\ln(x_S/x_N)$ vs 1000/T [f]		Thermodynamics of N ⇄ S equilibrium from van't Hoff plots [f, g]			Thermodynamics of N ⇄ S equilibrium from the average populations [h]
pD	PSEUROT analysis [e]	P_N	P_S	P_N	Ψ_m(N)	average slopes (σ)	average intercepts (σ)	ΔH° (σ)	-TΔS° (σ)	ΔG^{288} = ΔH°-TΔS°	ΔG^{288} = -0.288*R$\ln_{av}$ ($x_S/(x_N)$)
1.9	12911	-4° - 6°	122° - 165°	-3° - 5°	32° - 34°	-2.5 (0.5)	6.1 (1.8)	20.9 (4.5)	-14.7 (4.3)	6.2 (6.2)	6.3 (0.4)
2.2	12884	-3° - 6°	120° - 162°	-1° - 7°	31° - 34°	-2.2 (0.3)	5.1 (1.1)	18.0 (2.7)	-12.3 (2.6)	5.7 (3.7)	5.6 (0.3)
2.4	12806	-3° - 7°	122° - 158°	-1° - 8°	31° - 33°	-1.6 (0.2)	3.6 (0.7)	13.5 (1.6)	-8.7 (1.6)	4.8 (2.3)	4.8 (0.3)
2.5	12782	-3° - 6°	124° - 159°	-1° - 8°	31° - 33°	-1.5 (0.2)	3.4 (0.6)	12.7 (1.5)	-8.1 (1.5)	4.6 (2.1)	4.6 (0.2)
2.8	14206	-6° - 7°	120° - 155°	0° - 9°	29° - 33°	-1.0 (0.1)	1.9 (0.4)	8.5 (1.0)	-4.6 (0.9)	3.9 (1.3)	3.9 (0.3)
3.1	12703	-5° - 9°	120° - 155°	2° - 12°	29° - 32°	-0.8 (0.1)	1.5 (0.4)	6.9 (1.0)	-3.5 (1.0)	3.4 (1.4)	3.4 (0.3)
3.4	12978	-6° - 8°	123° - 154°	2° - 11°	29° - 32°	-0.6 (0.1)	0.7 (0.4)	4.8 (0.9)	-1.7 (0.9)	3.1 (1.3)	3.1 (0.3)
4.3	11275	-5° - 9°	123° - 152°	3° - 12°	29° - 32°	-0.5 (0.1)	0.4 (0.3)	3.6 (0.6)	-0.7 (0.6)	2.9 (0.9)	2.9 (0.3)
5.3	10207	-5° - 10°	123° - 150°	4° - 15°	29° - 32°	-0.5 (0.1)	0.5 (0.2)	4.1 (0.5)	-1.1 (0.5)	2.9 (0.7)	2.9 (0.3)
8.8	5960	-5° - 8°	124° - 149°	4° - 14°	29° - 32°	-0.4 (0.1)	0.2 (0.2)	3.2 (0.4)	-0.5 (0.4)	2.8 (0.6)	2.8 (0.3)
9.4	6631	-5° - 9°	129° - 149°	5° - 15°	29° - 32°	-0.3 (0.1)	0.0 (0.2)	2.5 (0.4)	0.0 (0.4)	2.5 (0.6)	2.5 (0.3)
9.8	9585	-5° - 9°	128° - 149°	5° - 15°	29° - 32°	-0.2 (0.1)	-0.1 (0.2)	1.8 (0.4)	0.3 (0.4)	2.1 (0.6)	2.1 (0.3)
10.4	9011	-5° - 9°	129° - 151°	5° - 15°	29° - 32°	-0.2 (0.1)	-0.3 (0.4)	1.3 (0.4)	0.6 (0.5)	2.0 (0.6)	2.0 (0.3)
11.0	10070	-5° - 9°	129° - 150°	5° - 15°	29° - 32°	-0.2 (0.1)	-0.2 (0.2)	1.4 (0.4)	0.4 (0.5)	1.8 (0.6)	1.8 (0.3)
11.6	9147	-5° - 9°	129° - 150°	5° - 16°	29° - 32°	-0.2 (0.1)	-0.1 (0.3)	1.5 (0.4)	0.3 (0.5)	1.8 (0.6)	1.8 (0.3)

[a] $^3J_{HH}$ at each of fifteen pDs at two extreme temperatures are given in Table 15. [b] Assuming Ψ_m (N) = Ψ_m (S), we have kept Ψ_m (N) and Ψ_m (S) fixed to identical values in the range from 30° to 34° for all pDs and surveyed the conformational hyperspace in 1° steps during several PSEUROT optimizations which resulted in different populations of N and S conformers with their distinctive P_N and P_S. [c] The error estimates of the PSEUROT analyses have been assessed in terms of ΔJ_{max} and r.m.s., both of which are reflecting the difference between $^3J_{calc}$ and $^3J_{exp}$ coupling constants. The number of successful PSEUROT analyses in column 2 are designated to those which were within the constrained values (see experimental section) as well as having a ΔJ_{max} and r.m.s. values smaller than 1.2 Hz and 0.8 Hz. [d] P_S of the minor S-type conformers were fixed at 160° ≤ P_S ≤ 180° in 10° steps with Ψ_m (S) being simultaneously fixed at 30°, 32° and 34°for all pDs during several PSEUROT optimizations which resulted in different populations of N and S conformers. [e] For each of these PSEUROT[9] calculations the coupling constants were 1000 times randomized which resulted in different populations of N and S conformers with their distinctive P_N and P_S (see experimental section). [f] The populations of N and S pseudorotamers obtained through each of the above PSEUROT calculations at different temperatures, shown in column 2, are the basis for the identical number of van't Hoff plots, which in turn were used to calculate the average slope and intercept. [g] The average of the slopes and the intercepts derived from all van't Hoff plots at a particular pD given in the columns 7 and 8 were finally used to calculate the average ΔH°, -TΔS° (at 288 K) and subsequently ΔG^{288} kJ/mol^{-1}) of N⇄ S equilibria of **4**. [h] ΔG^{288} calculated directly from the average logarithm $\ln_{av}$ (x_S/ (1- x_S)), by using the Gibbs equation ΔG^T = -(RT/1000)$\ln_{av}$ (x_S/ (1- x_S)) with 1- x_S = x_N, R is the gas constant and T is the temperature. The standard deviations are in parentheses.

Table 7. Pseudorotational analyses of temperature-dependent $^3J_{HH}$ (from 278 to 358K)[a] at 11 pDs (2.0 - 11.9) and determination of the pD-dependent thermodynamics of the two-state N ⇄ S equilibrium in 5'-OMe-β-D-ddG (**5**).

	Total number of PSEUROT	**Ψ_m constrained analyses in PSEUROT [b, c]**		**P_S and Ψ_m(S) constrained analyses in PSEUROT [c, d]**		**Slopes and intercepts of various van't Hoff plots from ln(x_S/x_N) vs 1000/T [f]**		**Thermodynamics of N ⇄ S equilibrium from van't Hoff plots [f, g]**			**Thermodynamics of N ⇄ S equilibrium from the average populations [h]**
pD	analyses [e]	P_N	P_S	P_N	Ψ_m(N)	average slopes (σ)	average intercepts (σ)	ΔH° (σ)	-TΔS° (σ)	ΔG^{288} = ΔH°-TΔS°	ΔG^{288} = -0.288*R$\ln_{av}$ (x_S/x_N)
2.0	12221	-2° - 7°	120° - 160°	-2° - 7°	31° - 33°	-2.36 (0.44)	5.70 (1.47)	19.6 (3.6)	-13.6 (3.5)	6.0 (5.1)	6.0 (0.3)
2.3	12619	-3° - 7°	120° - 160°	-1° - 7°	30° - 33°	-1.98 (0.30)	4.50 (1.00)	16.4 (2.5)	-10.8 (2.4)	5.7 (3.5)	5.6 (0.3)
2.7	12833	-1° - 9°	120° - 178°	2° - 10°	30° - 33°	-1.30 (0.16)	2.56 (0.51)	10.8 (1.3)	-6.1 (1.2)	4.7 (1.8)	4.6 (0.3)
3.1	12894	-3° - 21°	120° - 160°	3° - 13°	29° - 32°	-0.93 (0.13)	1.48 (0.42)	7.7 (1.1)	-3.5 (1.0)	4.2 (1.5)	4.1 (0.3)
3.6	12950	-7° - 9°	120° - 151°	0° - 13°	29° - 34°	-0.58 (0.11)	0.35 (0.37)	4.8 (0.9)	-0.8 (0.9)	4.0 (1.3)	4.0 (0.4)
5.2	13471	-6° - 9°	120° - 151°	3° - 12°	29° - 31°	-0.55 (0.06)	0.35 (0.20)	4.6 (0.5)	-0.8 (0.5)	3.8 (0.7)	3.8 (0.4)
8.8	13337	-6° - 9°	120° - 150°	4° - 13°	29° - 32°	-0.49 (0.06)	0.16 (0.21)	4.1 (0.5)	-0.4 (0.5)	3.7 (0.7)	3.8 (0.4)
9.3	13294	-5° - 10°	120° - 150°	5° - 14°	29° - 32°	-0.39 (0.06)	-0.10 (0.22)	3.3 (0.5)	0.2 (0.5)	3.5 (0.7)	3.5 (0.4)
10.0	13127	-7° - 10°	120° - 149°	4° - 15°	29° - 32°	-0.33 (0.06)	-0.28 (0.21)	2.7 (0.5)	0.7 (0.5)	3.4 (0.7)	3.3 (0.4)
10.9	12637	-7° - 10°	120° - 148°	4° - 15°	29° - 32°	-0.28 (0.06)	-0.40 (0.21)	2.4 (0.5)	1.0 (0.5)	3.3 (0.7)	3.3 (0.4)
11.9	12991	-6° - 11°	120° - 150°	5° - 16°	29° - 32°	-0.29 (0.07)	-0.37 (0.26)	2.4 (0.6)	0.9 (0.6)	3.3 (0.9)	3.3 (0.4)

[a] $^3J_{HH}$ at each of the eleven pDs at two extreme temperatures are given in Table 16. [b] Assuming $\Psi_m(N) = \Psi_m(S)$, we have kept $\Psi_m(N)$ and $\Psi_m(S)$ fixed to identical values in the range from 30° to 34° at each pD and surveyed the conformational hyperspace in 1° steps during several PSEUROT optimizations which resulted in different populations of N and S conformers with their distinctive P_N and P_S. [c] The error estimates of the PSEUROT analyses have been assessed in terms of ΔJ_{max} and r.m.s., both of which are reflecting the difference between $^3J_{calc}$ and $^3J_{exp}$ coupling constants. The number of successful PSEUROT analyses in column 2 are designated to those which were within the constrained values (see experimental section) as well as having a ΔJ_{max} and r.m.s. values smaller than 1.3 Hz and 0.8 Hz. [d] P_S of the minor S-type conformers were fixed at $160° \leq P_S \leq 180°$ in 10° steps with Ψ_m (S) being simultaneously fixed at 30°, 32°and 34°at each pD during several PSEUROT optimizations which resulted in different populations of N and S conformers. [e] For each of these PSEUROT[9] calculations the coupling constants were 1000 times randomized which resulted in different populations of N and S conformers with their respective P_N and P_S (see experimental section). [f] The populations of N and S pseudorotamers obtained through each of the above PSEUROT calculations at different temperatures, shown in column 2, are the basis for the identical number of van't Hoff plots, which in turn were used to calculate the average slopes and intercepts. [g] The average of the slopes and the intercepts derived from all van't Hoff plots at a particular pD given in the columns 7 and 8 were finally used to calculate the average ΔH°, -TΔS° (at 288 K) and subsequently ΔG^{288} (kJ/mol^{-1}) of N ⇄ S equilibria of **5**. [h] ΔG^{288} calculated directly from the average logarithm $\ln_{av}$ (x_S/ (1- x_S)), by using the Gibbs equation $\Delta G^T = -(RT/1000)\ln_{av}$ (x_S/ (1-x_S)) with 1- x_S − x_N , R is the gas constant and T is the temperature. The standard deviations are in parentheses.

Table 8. Pseudorotational analyses of temperature-dependent $^3J_{HH}$ (from 278 to 358 K)[a] at five pDs (1.5 - 6.4) and determination of the pD-dependent thermodynamics of the two-state N ⇄ S equilibrium in α-D-ddC (**6**).

		Ψ_m constrained analyses in PSEUROT [b, c]		**Slopes and intercepts of various van't Hoff plots from $\ln(x_S/x_N)$ vs 1000/T** [e]		**Thermodynamics of N ⇄ S equilibrium from van't Hoff plots** [e, f]			**Thermodynamics of N ⇄ S equilibrium from the average populations** [g]
pD	Total number of PSEUROT analyses [d]	P_N	P_S	average slopes (σ)	average intercepts (σ)	$\Delta H°$ (σ)	$-T\Delta S°$ (σ)	$\Delta G^{298} = \Delta H° - T\Delta S°$	$\Delta G^{298} = -0.298 * R\ln_{av}(x_S/x_N)$
1.5	7048	-19° - 5°	132° - 148°	0.34 (0.05)	-0.49 (0.19)	-2.8 (0.5)	1.2 (0.5)	-1.6 (0.7)	-1.6 (0.1)
2.0	7253	-18° - 10°	133° - 149°	0.36 (0.07)	-0.57 (0.22)	-3.0 (0.6)	1.4 (0.6)	-1.6 (0.8)	-1.6 (0.1)
3.7	2498	-23° - 10°	132° - 149°	0.35 (0.07)	-0.58 (0.23)	-2.9 (0.6)	1.4 (0.6)	-1.5 (0.8)	-1.5 (0.2)
4.4	3985	-27° - 2°	132° - 152°	0.38 (0.13)	-0.72 (0.44)	-3.1 (1.1)	1.8 (1.1)	-1.4 (1.5)	-1.4 (0.2)
6.4	4700	-18° - 8°	132° - 152°	0.31 (0.06)	-0.52 (0.19)	-2.5 (0.5)	1.3 (0.5)	-1.2 (0.7)	-1.2 (0.2)

[a] $^3J_{HH}$ at each of the five pDs at two extreme temperatures are given in Table 17. [b] Assuming $\Psi_m(N) = \Psi_m(S)$, we have kept $\Psi_m(N)$ and $\Psi_m(S)$ fixed to identical values in the range from 32° to 37° at each pD and surveyed the conformational hyperspace in 1° steps during several PSEUROT optimizations which resulted in different populations of N and S conformers with their distinctive P_N and P_S. [c] The error estimates of the PSEUROT analyses have been assessed in terms of ΔJ_{max} and r.m.s., both of which are reflecting the difference between $^3J_{calc}$ and $^3J_{exp}$ coupling constants. The number of successful PSEUROT analyses in column 2 are designated to those which were within the constrained values (see experimental section) as well as having a ΔJ_{max} and r.m.s. values smaller than 1.3 Hz and 0.8 Hz. [d] For each of these PSEUROT[9] calculations the coupling constants were 1000 times randomized which resulted in different populations of N and S conformers with their respective P_N and P_S (see experimental section). [e] The populations of N and S pseudorotamers obtained through each of the above PSEUROT calculations at different temperatures, shown in column 2, are the basis for the identical number of van't Hoff plots, which in turn were used to calculate the average slopes and intercepts. [f] The average of the slopes and the intercepts derived from all van't Hoff plots at a particular pD given in the columns 5 and 6 were finally used to calculate the average $\Delta H°$, $-T\Delta S°$ (at 298 K) and subsequently ΔG^{298} (kJ/mol^{-1}) of N ⇄ S equilibria of **6**. [g] ΔG^{298} calculated directly from the average logarithm $\ln_{av}(x_S/(1-x_S))$, by using the Gibbs equation $\Delta G^T = -(RT/1000)\ln_{av}(x_S/(1-x_N))$ with $1-x_S = x_N$, R is the gas constant and T is the temperature. The standard deviations are in parentheses.

Table 9. Pseudorotational analyses of temperature-dependent $^3J_{HH}$ (from 278 to 358 K)[a] at 10 pDs (1.1 - 6.6) and determination of the pD-dependent thermodynamics of the two-state N ⇄ S equilibrium in β-D-ddC (**7**).

	Total number of PSEUROT analyses [e]	Ψ_m constrained analyses in PSEUROT [b, c]		P_S and Ψ_m(S) constrained analyses in PSEUROT [c, d]		Slopes and intercepts of various van't Hoff plots from $\ln(x_S/x_N)$ vs 1000/T [f]		Thermodynamics of N ⇄ S equilibrium from van't Hoff plots [f, g]			Thermodynamics of N ⇄ S equilibrium from the average populations [h]
pD		P_N	P_S	P_N	Ψ_m(N)	average slopes (σ)	average intercepts (σ)	$\Delta H°$ (σ)	$-T\Delta S°$ (σ)	ΔG^{298} = $\Delta H°-T\Delta S°$	ΔG^{298} = $-0.298*R\ln_{av}(x_S/x_N)$
1.1	7337	2° - 18°	120° - 153°	7° - 16°	30° - 34°	-1.13 (0.17)	1.96 (0.53)	9.4 (1.4)	-4.9 (1.3)	4.5 (1.9)	4.4 (0.4)
1.9	7503	4° - 13°	120° - 154°	9° - 18°	30° - 34°	-1.12 (0.15)	2.03 (0.44)	9.7 (1.2)	-5.0 (1.1)	4.7 (1.6)	4.5 (0.4)
2.8	6840	5° - 14°	120° - 151°	10° - 19°	30° - 34°	-1.15 (0.14)	1.96 (0.43)	9.5 (1.2)	-4.9 (1.1)	4.6 (1.6)	4.7 (0.4)
3.2	6885	5° - 14°	120° - 151°	10° - 19°	30° - 34°	-1.07 (0.13)	1.77 (0.41)	8.9 (1.1)	-4.4 (1.0)	4.5 (1.5)	4.6 (0.4)
3.6	5857	4° - 13°	120° - 152°	9° - 18°	30° - 34°	-0.96 (0.12)	1.47 (0.40)	8.0 (1.0)	-3.6 (1.0)	4.4 (1.4)	4.3 (0.4)
4.1	6819	4° - 15°	120° - 153°	9° - 21°	30° - 34°	-0.89 (0.11)	1.37 (0.36)	7.4 (0.9)	-3.4 (0.9)	4.0 (1.3)	4.0 (0.4)
4.5	7564	4° - 16°	120° - 154°	10° - 20°	30° - 34°	-0.87 (0.11)	1.34 (0.35)	7.2 (0.9)	-3.3 (0.9)	3.9 (1.3)	3.9 (0.4)
5.2	4071	5° - 16°	120° - 148°	12° - 22°	29° - 33°	-0.81 (0.09)	1.24 (0.28)	6.7 (0.7)	-3.1 (0.7)	3.6 (1.0)	3.6 (0.4)
5.7	7223	7° - 18°	120° - 148°	15° - 25°	29° - 34°	-0.78 (0.09)	1.23 (0.30)	6.5 (0.7)	-3.0 (0.7)	3.5 (1.0)	3.5 (0.4)
6.6	5864	7° - 19°	120° - 148°	15° - 26°	30° - 34°	-0.80 (0.08)	1.30 (0.30)	6.6 (0.7)	-3.2 (0.7)	3.4 (1.0)	3.4 (0.4)

[a] $^3J_{HH}$ at each of the ten pDs at two extreme temperatures are given in Table 18. [b] Assuming $\Psi_m(N) = \Psi_m(S)$, we have kept $\Psi_m(N)$ and $\Psi_m(S)$ fixed to identical values in the range from 30° to 34° at each pD < 4.5 and from 30° to 35° at pD > 4.5 and surveyed the conformational hyperspace in 1° steps during several PSEUROT optimizations which resulted in different populations of N and S conformers with their distinctive P_N and P_S. [c] The error estimates of the PSEUROT analyses have been assessed in terms of ΔJ_{max} and r.m.s., both of which are reflecting the difference between $^3J_{calc}$ and $^3J_{exp}$ coupling constants. The number of successful PSEUROT analyses in column 2 are designated to those which were within the constrained values (see experimental section) as well as having a ΔJ_{max} and r.m.s. values smaller than 1.2 Hz and 0.8 Hz. [d] P_S of the minor S-type conformers were fixed at $160° \leq P_S \leq 180°$ in 10° steps with Ψ_m (S) being simultaneously fixed at 30°and 34°at each pD during several PSEUROT optimizations which resulted in different populations of N and S conformers. [e] For each of these PSEUROT[9] calculations the coupling constants were 1000 times randomized which resulted in different populations of N and S conformers with their respective P_N and P_S (see experimental section). [f] The populations of N and S pseudorotamers obtained through each of the above PSEUROT calculations at different temperatures, shown in column 2, are the basis for the identical number of van't Hoff plots, which in turn were used to calculate the average slopes and intercepts. [g] The average of the slopes and the intercepts derived from all van't Hoff plots at a particular pD given in the columns 7 and 8 were finally used to calculate the average $\Delta H°$, $-T\Delta S°$ (at 298 K) and subsequently ΔG^{298} (kJ/mol^{-1}) of N⇄ S equilibria of 7. [h] ΔG^{298} calculated directly from the average logarithm $\ln_{av}$ (x_S/ (1- x_S)), by using the Gibbs equation $\Delta G^T = -(RT/1000)\ln_{av}(x_S/(1-x_S))$ with $1-x_S = x_N$, R is the gas constant and T is the temperature. The standard deviations are in parentheses.

Table 10. Pseudorotational analyses of temperature-dependent $^3J_{HH}$ (from 278 to 358 K)[a] at eight pDs (6.5 - 11.7) and determination of the pD-dependent thermodynamics of the two-state N ⇄ S equilibrium in α-D-ddT (**8**).

		Ψ_m constrained analyses in PSEUROT [b, c]		**Slopes and intercepts of various van't Hoff plots from $\ln(x_S/x_N)$ vs 1000/T** [e]		**Thermodynamics of N ⇄ S equilibrium from van't Hoff plots** [e, f]			**Thermodynamics of N ⇄ S equilibrium from the average populations** [g]
pD	Total number of PSEUROT analyses [d]	P_N	P_S	average slopes (σ)	average intercepts (σ)	$\Delta H°$ (σ)	$-T\Delta S°$ (σ)	$\Delta G^{298} = \Delta H° - T\Delta S°$	$\Delta G^{298} = -0.298 * R\ln_{av}(x_S/x_N)$
6.5	11087	-23° - 7°	126° - 151°	0.13 (0.07)	-0.26 (0.24)	-1.1 (0.6)	0.6 (0.6)	-0.5 (0.8)	-0.5 (0.2)
8.5	9717	-23° - 6°	126° - 151°	0.14 (0.07)	-0.28 (0.23)	-1.2 (0.6)	0.7 (0.6)	-0.5 (0.8)	-0.5 (0.2)
9.0	8520	-23° - 4°	126° - 149°	0.11 (0.06)	-0.19 (0.19)	-0.9 (0.5)	0.5 (0.5)	-0.4 (0.7)	-0.4 (0.2)
9.5	12528	-22° - 6°	126° - 150°	0.12 (0.06)	-0.22 (0.20)	-1.0 (0.5)	0.6 (0.5)	-0.4 (0.7)	-0.4 (0.2)
10.0	11424	-20° - 6°	126° - 151°	0.10 (0.06)	-0.21 (0.19)	-0.8 (0.5)	0.5 (0.5)	-0.3 (0.7)	-0.4 (0.2)
10.5	12686	-21° - 4°	126° - 151°	0.06 (0.06)	-0.09 (0.19)	-0.5 (0.5)	0.2 (0.5)	-0.2 (0.7)	-0.2 (0.2)
10.8	13471	-22° - 4°	126° - 151°	0.07 (0.06)	-0.12 (0.19)	-0.5 (0.5)	0.3 (0.5)	-0.2 (0.7)	-0.2 (0.2)
11.7	13145	-21° - 4°	126° - 152°	0.08 (0.06)	-0.16 (0.19)	-0.6 (0.5)	0.4 (0.5)	-0.2 (0.7)	-0.2 (0.2)

[a] $^3J_{HH}$ at each of the eight pDs at two extreme temperatures are given in Table 19. [b] Assuming $\Psi_m(N) = \Psi_m(S)$, we have kept $\Psi_m(N)$ and $\Psi_m(S)$ fixed to identical values in the range from 31° to 37° at each pD and surveyed the conformational hyperspace in 1° steps during several PSEUROT optimizations which resulted in different populations of N and S conformers with their distinctive P_N and P_S. [c] The error estimates of the PSEUROT analyses have been assessed in terms of ΔJ_{max} and r.m.s., both of which are reflecting the difference between $^3J_{calc}$ and $^3J_{exp}$ coupling constants. The number of successful PSEUROT analyses in column 2 are designated to those which were within the constrained values (see experimental section) as well as having a ΔJ_{max} and r.m.s. values smaller than 1.3 Hz and 0.8 Hz. [d] For each of these PSEUROT[9] calculations the coupling constants were 1000 times randomized which resulted in different populations of N and S conformers with their respective P_N and P_S (see experimental section). [e] The populations of N and S pseudorotamers obtained through each of the above PSEUROT calculations at different temperatures, shown in column 2, are the basis for the identical number of van't Hoff plots, which in turn were used to calculate the average slopes and intercepts. [f] The average of the slopes and the intercepts derived from all van't Hoff plots at a particular pD given in the columns 5 and 6 were finally used to calculate the average $\Delta H°$, $-T\Delta S°$ (at 298 K) and subsequently ΔG^{298} (kJ/mol^{-1}) of N ⇄ S equilibria of **8**. [g] ΔG^{298} calculated directly from the average logarithm $\ln_{av}(x_S/(1-x_S))$, by using the Gibbs equation $\Delta G^T = -(RT/1000)\ln_{av}(x_S/(1-x_S))$ with $1-x_S = x_N$, R is the gas constant and T is the temperature. The standard deviations are in parentheses.

Table 11. Pseudorotational analyses of temperature-dependent $^3J_{HH}$ (from 278 to 358 K)[a] at eight pDs (6.8 - 11.4) and determination of the pD-dependent thermodynamics of the two-state N ⇄ S equilibrium in β-D-ddT (**9**).

	Total number of PSEUROT	Ψ_m constrained analyses in PSEUROT [b, c]		P_S and $\Psi_m(S)$ constrained analyses in PSEUROT [c, d]		Slopes and intercepts of various van't Hoff plots from $\ln(x_S/x_N)$ vs 1000/T [f]		Thermodynamics of N ⇄ S equilibrium from van't Hoff plots [f, g]			Thermodynamics of N ⇄ S equilibrium from the average populations [h]
pD	analyses [e]	P_N	P_S	P_N	$\Psi_m(N)$	average slopes (σ)	average intercepts (σ)	ΔH° (σ)	-TΔS° (σ)	ΔG^{298} = ΔH°-TΔS°	ΔG^{298} = -0.298*R$\ln_{av}(x_S/x_N)$
6.8	12388	8° - 22°	120° - 146°	18° - 29°	29° - 32°	-0.65 (0.08)	0.90 (0.27)	5.4 (0.7)	-2.2 (0.7)	3.2 (1.0)	3.1 (0.5)
7.8	11287	7° - 22°	120° - 146°	17° - 29°	29° - 32°	-0.65 (0.08)	0.90 (0.27)	5.4 (0.7)	-2.2 (0.7)	3.1 (1.0)	3.1 (0.5)
8.7	12830	7° - 23°	120° - 145°	17° - 28°	29° - 32°	-0.62 (0.08)	0.83 (0.26)	5.1 (0.7)	-2.1 (0.6)	3.1 (0.9)	3.1 (0.5)
9.2	12904	6° - 23°	120° - 146°	17° - 29°	29° - 32°	-0.61 (0.09)	0.82 (0.29)	5.0 (0.7)	-2.0 (0.7)	3.0 (1.0)	3.0 (0.5)
9.8	8698	10° - 25°	120° - 148°	19° - 30°	29° - 33°	-0.51 (0.08)	0.57 (0.25)	4.3 (0.6)	-1.4 (0.6)	2.9 (0.9)	2.8 (0.4)
10.3	3832	9° - 26°	120° - 143°	20° - 33°	29° - 32°	-0.47 (0.08)	0.53 (0.27)	3.9 (0.7)	-1.3 (0.7)	2.6 (0.9)	2.6 (0.5)
10.9	14173	11° - 27°	120° - 145°	23° - 35°	29° - 33°	-0.46 (0.09)	0.50 (0.30)	3.8 (0.7)	-1.3 (0.8)	2.5 (1.0)	2.5 (0.4)
11.4	11494	14° - 28°	121° - 146°	24° - 36°	29° - 33°	-0.43 (0.07)	0.46 (0.25)	3.6 (0.6)	-1.1 (0.6)	2.5 (0.9)	2.4 (0.4)

[a] $^3J_{HH}$ at each of the eight pDs at two extreme temperatures are given in Table 20. [b] Assuming $\Psi_m(N) = \Psi_m(S)$, we have kept $\Psi_m(N)$ and $\Psi_m(S)$ fixed to identical values in the range from 30° to 34° at each pD and surveyed the conformational hyperspace in 1° steps during several PSEUROT optimizations which resulted in different populations of N and S conformers with their distinctive P_N and P_S. [c] The error estimates of the PSEUROT analyses have been assessed in terms of ΔJ_{max} and r.m.s., both of which are reflecting the difference between $^3J_{calc}$ and $^3J_{exp}$ coupling constants. The number of successful PSEUROT analyses in column 2 are designated to those which were within the constrained values (see experimental section) as well as having a ΔJ_{max} and r.m.s. values smaller than 1.3 Hz and 0.8 Hz. [d] P_S of the minor S-type conformers were fixed at $160° \leq P_S \leq 180°$ in 10° steps with Ψ_m (S) being simultaneously fixed at 30°, 32° and 34°at each pD during several PSEUROT optimizations which resulted in different populations of N and S conformers. [e] For each of these PSEUROT[9] calculations the coupling constants were 1000 times randomized which resulted in different populations of N and S conformers with their respective P_N and P_S (see experimental section). [f] The populations of N and S pseudorotamers obtained through each of the above PSEUROT calculations at different temperatures, shown in column 2, are the basis for the identical number of van't Hoff plots, which in turn were used to calculate the average slopes and intercepts. [g] The average of the slopes and the intercepts derived from all van't Hoff plots at a particular pD given in the columns 7 and 8 were finally used to calculate the average ΔH°, -TΔS° (at 298 K) and subsequently ΔG^{298} (kJ/mol^{-1}) of N ⇄ S equilibria of **9**. [h] ΔG^{298} calculated directly from the average logarithm $\ln_{av}$ (x_S/ (1- x_S)), by using the Gibbs equation $\Delta G^T = -(RT/1000)\ln_{av}$ (x_S/ (1- x_S)) with 1- x_S = x_N, R is the gas constant and T is the temperature. The standard deviations are in parentheses.

Table 12. The temperature-dependent vicinal coupling constants in α-D-ddA (**1**) as a function of pD[a]

	α-D-ddA (**1**)															
pD	$^3J_{1'2'}$		$^3J_{1'2''}$		$^3J_{2'3'}$		$^3J_{2'3''}$		$^3J_{2''3'}$		$^3J_{2''3''}$		$^3J_{3'4'}$		$^3J_{3''4'}$	
	278 K	358 K	278 K	358 K	278 K	358 K	278 K	358 K	278 K	358 K	278 K	358 K	278 K	358 K	278 K	358 K
1.5[b]	6.7	6.8	3.6	3.7	9.1	9.1	7.5	7.4	5.8	6.0	8.2	8.3	6.3	6.4	7.5	7.4
2.0[b]	6.7	6.8	3.6	3.7	9.1	9.2	7.5	7.4	5.8	5.9	8.2	8.3	6.3	6.6	7.6	7.3
3.2[c]	6.7	6.6	3.6	3.8	9.1	9.2	7.5	7.2	5.9	6.1	8.4	8.4	6.3	6.5	7.6	7.5
3.6[c]	6.6	6.6	3.7	3.9	9.1	9.2	7.5	7.1	5.9	6.1	8.4	8.4	6.3	6.6	7.6	7.4
4.0[d]	6.6	6.6	3.8	4.1	9.1	9.2	7.3	6.9	5.9	6.2	8.4	8.4	6.3	6.6	7.6	7.3
6.8	6.6	6.6	3.8	4.1	9.1	9.2	7.3	6.9	5.9	6.2	8.4	8.4	6.3	6.6	7.6	7.3

[a] In Hz, error ± 0.1 Hz for $^3J_{1'2''}$ and $^3J_{1'2''}$, 0.2 Hz for all other $^3J_{HH}$. Only $^3J_{HH}$ at the lowest and the highest temperature are tabulated, whereas they are available at several intermediate temperatures in 5 K or 10 K steps. Note that the complete set of $^3J_{HH}$ between the two extreme temperatures at each pD have been used in the calculation of thermodynamic quantities through pseudorotational analyses and van't Hoff plots. Tabulated coupling constants are the result of simulation and iteration procedure by DAISY program.[16] [b] At 274 K and 304 K. [c] At 278 K and 328 K. [d] At 278 K and 348 K.

Table 13. The temperature-dependent vicinal coupling constants in β-D-ddA (**2**) as a function of pD[a]

	β-D-ddA (**2**)															
pD	$^3J_{1'2'}$		$^3J_{1'2''}$		$^3J_{2'3'}$		$^3J_{2'3''}$		$^3J_{2''3'}$		$^3J_{2''3''}$		$^3J_{3'4'}$		$^3J_{3''4'}$	
	278 K	358 K	278 K	358 K	278 K	358 K	278 K	358 K	278 K	358 K	278 K	358 K	278 K	358 K	278 K	358 K
1.6[b]	2.4	2.6	7.0	7.0	7.9	8.0	2.7	3.1	11.1	10.9	8.2	8.1	9.5	9.2	6.3	6.4
2.1[c]	2.4	2.7	7.0	7.0	7.9	8.0	2.7	3.1	11.1	10.8	8.2	8.3	9.4	9.1	6.3	6.4
2.6[d]	2.5	2.9	7.0	7.0	8.0	8.0	2.9	3.4	11.0	10.5	8.1	8.3	9.4	8.9	6.3	6.5
3.4[e]	2.7	3.3	7.0	7.0	7.9	8.0	3.2	3.8	10.8	10.1	8.0	8.2	9.2	8.6	6.5	6.6
4.0[e]	3.0	3.5	6.9	6.9	7.9	7.9	3.5	4.0	10.4	9.9	8.1	8.3	9.0	8.6	6.5	6.6
4.5[f]	3.2	3.7	6.9	6.9	7.9	8.2	3.7	4.2	10.1	9.5	8.2	8.3	8.8	8.2	6.5	6.7
5.0[f]	3.2	3.7	6.9	6.9	8.0	8.3	3.8	4.3	10.2	9.4	8.1	8.3	8.8	8.3	6.5	6.7
5.5	3.2	3.8	6.9	6.9	8.0	8.3	3.8	4.4	10.2	9.3	8.1	8.3	8.7	8.1	6.5	6.8
6.7	3.2	3.8	6.9	6.9	8.1	8.3	3.8	4.4	10.2	9.3	8.1	8.3	8.7	8.2	6.6	6.7

[a] In Hz, Only $^3J_{HH}$ at the lowest and the highest temperature are tabulated, whereas they are available at several intermediate temperatures in 5 K steps. Note that the complete set of $^3J_{HH}$ between 274 and 358 K at each pD have been used in the calculation of thermodynamic quantities through pseudorotational analyses and van't Hoff plots. Tabulated coupling constants are the result of simulation and iteration procedure by DAISY program[16]. [b] $^3J_{HH}$ determined between 274 and 294 K because of decomposition at higher temperatures. [c] $^3J_{HH}$ determined between 274 and 299 K because of decomposition at higher temperatures. [d] $^3J_{HH}$ determined between 278 and 313 K because of decomposition at higher temperatures. [e] $^3J_{HH}$ determined between 278 and 328 K because of decomposition at higher temperatures. [f] $^3J_{HH}$ determined between 278 and 348K.

Table 14. The temperature-dependent vicinal coupling constants in α-D-ddG (**3**) as a function of pD[a]

	α-D-ddG (**3**)															
pD	$^3J_{1'2'}$		$^3J_{1'2''}$		$^3J_{2'3'}$		$^3J_{2'3''}$		$^3J_{2''3'}$		$^3J_{2''3''}$		$^3J_{3'4'}$		$^3J_{3''4'}$	
	278 K	358 K	278 K	358 K	278 K	358 K	278 K	358 K	278 K	358 K	278 K	358 K	278 K	358 K	278 K	358 K
2.2[b]	6.5	6.5	2.8	3.2	9.1	9.1	8.5	8.1	4.8	5.3	8.4	8.5	5.3	5.8	8.0	7.7
2.4[c]	6.5	6.6	3.0	3.4	9.2	9.1	8.3	7.9	5.0	5.5	8.4	8.5	5.5	5.9	7.9	7.7
2.7[b]	6.6	6.6	3.3	3.7	9.0	9.1	8.1	7.4	5.5	5.9	8.3	8.5	5.8	6.3	7.8	7.6
3.0[c]	6.6	6.7	3.6	3.9	9.1	9.2	7.6	7.3	5.7	6.0	8.4	8.4	6.1	6.4	7.7	7.5
3.4[d]	6.7	6.7	3.9	4.1	9.1	9.2	7.3	7.1	6.0	6.2	8.5	8.5	6.5	6.5	7.5	7.5
4.2[e]	6.7	6.7	4.0	4.1	9.1	9.2	7.1	7.0	6.2	6.3	8.5	8.5	6.7	6.7	7.4	7.4
8.7	6.7	6.7	4.1	4.2	9.1	9.2	7.2	6.7	6.2	6.3	8.4	8.5	6.7	6.7	7.2	7.4
9.2	6.6	6.7	4.2	4.2	8.2	9.2	7.1	6.9	6.3	6.3	8.4	8.5	6.8	6.7	7.4	7.4
9.6	6.6	6.7	4.2	4.3	9.2	9.2	6.9	6.8	6.3	6.3	8.4	8.5	6.7	6.6	7.4	7.3
11.8	6.6	6.6	4.3	4.3	9.1	9.2	7.0	6.8	6.4	6.4	8.4	8.5	6.7	6.7	7.4	7.3

[a] In Hz, error ± 0.2 Hz for $^3J_{3'4'}$ and $^3J_{3''4'}$, 0.1 Hz for all other $^3J_{HH}$. Only $^3J_{HH}$ at the lowest and the highest temperature are tabulated, whereas they are available at several intermediate temperatures in 5 K or 10 K steps. Note that the complete set of $^3J_{HH}$ between the two extreme temperatures at each pD have been used in the calculation of thermodynamic quantities through pseudorotational analyses and van't Hoff plots. Tabulated coupling constants are the result of simulation and iteration procedure by DAISY program.[16] [b] At 274 K and 303 K. [c] At 274 K and 298 K. [d] At 278 K and 313 K. [e] At 278 K and 328 K.

Table 15. The temperature-dependent vicinal coupling constants in β-D-ddG (**4**) as a function of pD[a]

	β-D-ddG (**4**)															
pD	$^3J_{1'2'}$		$^3J_{1'2''}$		$^3J_{2'3'}$		$^3J_{2'3''}$		$^3J_{2''3'}$		$^3J_{2''3''}$		$^3J_{3'4'}$		$^3J_{3''4'}$	
	278 K	358 K	278 K	358 K	278 K	358 K	278 K	358 K	278 K	358 K	278 K	358 K	278 K	358 K	278 K	358 K
1.9[b]	1.6	2.1	6.7	6.8	7.5	7.6	1.9	2.5	12.0	11.5	7.7	8.0	10.1	9.6	6.0	6.1
2.2[c]	1.6	2.3	6.8	6.8	7.5	7.8	2.1	2.8	11.9	11.3	7.8	8.2	10.0	9.5	6.0	6.1
2.4[c]	1.9	2.7	6.8	6.9	7.7	7.8	2.5	3.2	11.5	10.8	8.0	8.1	9.8	9.3	6.1	6.3
2.5[c]	2.0	2.7	6.8	6.9	7.6	7.9	2.6	3.1	11.6	10.7	7.9	8.2	9.7	9.2	6.1	6.4
2.8[d]	2.5	3.1	6.9	6.9	7.9	8.0	2.9	3.5	11.1	10.3	8.0	8.3	9.3	8.9	6.3	6.5
3.1[e]	2.8	3.2	7.0	7.0	8.0	8.2	3.2	3.7	10.7	10.2	8.1	8.3	9.0	8.7	6.4	6.5
3.4[c]	2.9	3.4	6.9	7.0	8.0	8.2	3.4	3.8	10.4	10.0	8.1	8.2	8.9	8.6	6.4	6.6
4.3[e]	3.1	3.6	7.0	7.0	8.1	8.3	3.6	4.1	10.1	9.8	8.1	8.4	8.8	8.4	6.5	6.7
5.3[f]	3.2	3.8	6.9	7.0	8.0	8.4	3.7	4.3	10.2	9.4	8.1	8.5	8.7	8.3	6.5	6.7
8.8	3.4	3.8	6.9	7.0	8.1	8.3	3.9	4.4	10.1	9.4	8.3	8.4	8.6	8.2	6.5	6.8
9.4	3.5	3.9	7.0	7.0	8.1	8.3	4.0	4.5	9.7	9.3	8.5	8.4	8.6	8.1	6.5	6.8
9.8	3.8	4.1	6.9	6.9	8.1	8.3	4.4	4.6	9.4	9.0	8.3	8.4	8.3	8.0	6.8	6.9
10.4[g]	3.9	4.1	6.9	7.0	8.1	8.3	4.5	4.7	9.2	9.0	8.3	8.4	8.2	7.9	6.8	6.9
11.0[g]	4.0	4.2	6.9	6.9	8.3	8.3	4.6	4.9	9.1	8.8	8.2	8.4	8.1	7.9	6.9	6.9
11.6[g]	4.0	4.3	6.9	6.9	83	8.3	4.7	4.9	9.1	8.8	8.2	8.4	8.1	7.9	7.0	6.9

[a] In Hz, Only $^3J_{HH}$ at the lowest and the highest temperature are tabulated, whereas they are available at several intermediate temperatures in 5 K steps. Note that the complete set of $^3J_{HH}$ between 274 and 358 K at each pD have been used in the calculation of thermodynamic quantities through pseudorotational analyses and van't Hoff plots. Tabulated coupling constants are the result of simulation and iteration procedure by DAISY program[16]. [b] $^3J_{HH}$ determined between 274 and 303 K because of decomposition at higher temperatures. [c] $^3J_{HH}$ determined between 274 and 308 K because of decomposition at higher temperatures. [d] $^3J_{HH}$ determined between 274 and 313 K because of decomposition at higher temperatures. [e] $^3J_{HH}$ determined between 278 and 328 K because of decomposition at higher temperatures. [f] $^3J_{HH}$ determined between 278 and 348 K. [g] $^3J_{HH}$ determined between 288 and 358 K because H2' and H2'' are almost isochronous at 278 K.

Table 16. The temperature-dependent vicinal coupling constants in 5'-OMe-β-D-ddG (**5**) as a function of pD[a]

	5'-OMe-β-D-ddG (**5**)															
pD	$^3J_{1'2'}$		$^3J_{1'2"}$		$^3J_{2'3'}$		$^3J_{2'3"}$		$^3J_{2"3'}$		$^3J_{2"3"}$		$^3J_{3'4'}$		$^3J_{3"4'}$	
	278 K	358 K	278 K	358 K	278 K	358 K	278 K	358 K	278 K	358 K	278 K	358 K	278 K	358 K	278 K	358 K
2.0[b]	1.7	2.1	6.8	6.9	7.6	7.7	2.0	2.5	12.0	11.3	8.0	8.1	10.1	9.7	6.0	6.2
2.3[c]	1.8	2.3	6.9	6.9	7.6	7.8	2.1	2.7	11.8	11.2	8.0	8.2	9.9	9.5	6.1	6.2
2.7[d]	2.2	2.8	6.9	7.0	7.8	7.9	2.4	3.2	11.4	10.7	8.1	8.3	9.8	9.2	6.2	6.3
3.1[e]	2.5	2.9	7.1	7.1	7.9	8.0	2.8	3.3	11.0	10.6	8.2	8.4	9.5	9.0	6.3	6.5
3.6[f]	2.7	3.1	7.2	7.1	8.0	8.1	3.0	3.4	10.9	10.4	8.3	8.4	9.1	8.8	6.4	6.6
5.2	2.8	3.3	7.1	7.1	8.1	8.2	3.1	3.8	10.7	10.0	8.3	8.4	9.1	8.6	6.4	6.6
8.8	2.9	3.3	7.1	7.1	8.1	8.1	3.1	3.7	10.7	10.0	8.3	8.4	9.0	8.7	6.5	6.6
9.3	3.0	3.4	7.1	7.1	8.1	8.1	3.3	3.7	10.6	10.0	8.3	8.4	8.9	8.7	6.4	6.6
10.0	3.1	3.4	7.1	7.0	8.1	8.2	3.2	3.7	10.6	10.0	8.3	8.4	8.9	8.7	6.5	6.7
10.9	3.1	3.4	7.1	7.0	8.1	8.3	3.3	3.7	10.5	10.0	8.4	8.4	8.9	8.7	6.6	6.6
11.9[g]	3.1	3.4	7.1	7.1	8.1	8.3	3.3	3.7	10.4	10.0	8.3	8.4	8.9	8.7	6.5	6.6

[a] In Hz, error ± 0.2 Hz for $^3J_{3'4'}$ and $^3J_{3"4'}$, 0.1 Hz for all other $^3J_{HH}$. Only $^3J_{HH}$ at the lowest and the highest temperature are tabulated, whereas they are available at several intermediate temperatures in 5 K or 10 K steps. Note that the complete set of $^3J_{HH}$ between the two extreme temperatures at each pD have been used in the calculation of thermodynamic quantities through pseudorotational analyses and van't Hoff plots. Tabulated coupling constants are the result of simulation and iteration procedure by DAISY program.[16] [b] At 274 K and 303 K. [c] At 274 K and 308 K. [d] At 274 K and 313 K. [e] At 274 K and 318 K. [f] At 278 K and 328 K. [g] At 278 K and 348 K.

Table 17. The temperature-dependent vicinal coupling constants in α-D-ddC (**6**) as a function of pD[a]

	α-D-ddC (**6**)															
pD	$^3J_{1'2'}$		$^3J_{1'2"}$		$^3J_{2'3'}$		$^3J_{2'3"}$		$^3J_{2"3'}$		$^3J_{2"3"}$		$^3J_{3'4'}$		$^3J_{3"4'}$	
	278 K	358 K	278 K	358 K	278 K	358 K	278 K	358 K	278 K	358 K	278 K	358 K	278 K	358 K	278 K	358 K
1.5[b]	6.3	6.5	3.5	3.8	8.6	8.9	8.0	7.2	5.5	6.2	8.1	8.4	5.7	6.1	7.6	7.4
2.0[c]	6.4	6.4	3.5	3.9	8.5	8.8	7.8	7.5	5.5	6.2	8.1	8.3	5.5	6.0	7.7	7.3
3.7[b]	6.3	6.5	3.5	3.9	8.6	8.9	8.0	7.3	5.7	6.3	8.2	8.5	5.5	6.1	7.6	7.3
4.4[d]	6.3	6.4	3.7	3.9	8.7	8.6	7.8	7.1	5.9	6.2	8.3	8.4	5.5	5.8	7.6	7.4
6.4	6.4	6.5	3.8	4.3	8.6	8.8	7.8	7.1	5.8	6.6	8.3	8.5	5.8	6.2	7.1	7.0

[a] In Hz, error ± 0.2 Hz. Only $^3J_{HH}$ at the lowest and the highest temperature are tabulated, whereas they are available at several intermediate temperatures in 10 K steps. Note that the complete set of $^3J_{HH}$ between the two extreme temperatures at each pD have been used in the calculation of thermodynamic quantities through pseudorotational analyses and van't Hoff plots. Tabulated coupling constants are the result of simulation and iteration procedure by DAISY program.[16] [b] At 278 K and 348 K. [c] At 278 K and 338 K. [d] At 278 K and 318 K. $^3J_{HH}$ could not be extracted above 318K at this pD due to strongly coupled system.

Table 18. The temperature-dependent vicinal coupling constants in β-D-ddC (**7**) as a function of pD[a]

	β-D-ddC (**7**)															
pD	$^3J_{1'2'}$		$^3J_{1'2''}$		$^3J_{2'3'}$		$^3J_{2'3''}$		$^3J_{2''3'}$		$^3J_{2''3''}$		$^3J_{3'4'}$		$^3J_{3''4'}$	
	278 K	358 K	278 K	358 K	278 K	358 K	278 K	358 K	278 K	358 K	278 K	358 K	278 K	358 K	278 K	358 K
1.1[b]	2.3	3.0	6.9	6.9	7.9	8.3	2.6	3.4	11.4	10.4	7.9	8.2	10.0	9.3	5.8	6.2
1.9[c]	2.3	3.2	6.9	6.9	7.8	8.1	2.5	3.5	11.4	10.3	8.0	8.2	10.1	9.2	5.7	6.2
2.8[c]	2.3	3.2	6.9	7.0	7.9	8.3	2.5	3.6	11.3	10.2	8.1	8.3	10.1	9.2	5.8	6.2
3.2[c]	2.3	3.2	7.0	7.0	7.9	8.3	2.6	3.6	11.2	10.3	8.1	8.2	10.0	9.2	5.8	6.3
3.6[c]	2.4	3.2	6.9	7.0	7.8	8.3	2.7	3.7	11.3	10.3	7.9	8.2	9.8	9.1	5.8	6.2
4.1[c]	2.6	3.4	7.0	7.0	8.0	8.3	2.8	3.7	11.0	10.1	7.9	8.2	9.7	9.0	5.8	6.2
4.5[c]	2.7	3.5	6.9	7.0	8.0	8.3	2.8	3.9	11.0	9.9	7.9	8.2	9.6	9.1	5.9	6.1
5.2	2.9	3.8	7.0	6.9	8.1	8.4	3.1	4.1	10.7	9.7	8.0	8.3	9.7	8.7	5.9	6.3
5.7	2.9	3.8	7.1	7.0	8.2	8.5	3.1	4.1	10.6	9.4	7.8	8.4	9.6	8.9	5.9	6.4
6.6	3.0	3.8	7.0	6.9	8.0	8.5	3.1	4.1	10.7	9.3	7.9	8.4	9.6	8.9	5.9	6.4

[a] In Hz, error ± 0.1 Hz for $^3J_{1'2'}$ and $^3J_{1'2''}$, 0.2 Hz for all other $^3J_{HH}$. Only $^3J_{HH}$ at the lowest and the highest temperature are tabulated, whereas they are available at several intermediate temperatures in 5 K or 10 K steps. Note that the complete set of $^3J_{HH}$ between the two extreme temperatures at each pD have been used in the calculation of thermodynamic quantities through pseudorotational analyses and van't Hoff plots. Tabulated coupling constants are the result of simulation and iteration procedure by DAISY program.[16] [b] At 278 K and 338 K. [c] At 278 K and 348 K.

Table 19. The temperature-dependent vicinal coupling constants in α-D-ddT (**8**) as a function of pD[a]

	α-D-ddT (**8**)															
pD	$^3J_{1'2'}$		$^3J_{1'2''}$		$^3J_{2'3'}$		$^3J_{2'3''}$		$^3J_{2''3'}$		$^3J_{2''3''}$		$^3J_{3'4'}$		$^3J_{3''4'}$	
	278 K	358 K	278 K	358 K	278 K	358 K	278 K	358 K	278 K	358 K	278 K	358 K	278 K	358 K	278 K	358 K
6.5[b]	6.5	6.6	4.6	4.8	8.7	8.8	6.6	6.2	7.0	7.1	8.4	8.6	6.4	6.6	7.1	7.0
8.5[b]	6.5	6.6	4.6	4.8	8.7	8.9	6.6	6.2	6.9	7.1	8.4	8.6	6.4	6.6	7.0	7.1
9.0[b]	6.5	6.7	4.7	4.9	8.7	8.8	6.5	6.3	7.0	7.2	8.5	8.6	6.5	6.7	7.1	7.0
9.5	6.5	6.6	4.7	4.9	8.7	8.8	6.6	6.2	6.9	7.2	8.4	8.6	6.5	6.7	7.1	7.0
10.0	6.5	6.6	4.9	5.0	8.6	8.8	6.5	6.2	7.1	7.2	8.3	8.6	6.6	6.8	7.1	7.0
10.5	6.5	6.6	4.9	5.1	8.6	8.8	6.4	6.2	7.1	7.3	8.4	8.6	6.7	6.7	7.0	7.0
10.8	6.5	6.6	4.9	5.1	8.6	8.7	6.4	6.2	7.1	7.3	8.4	8.5	6.7	6.7	7.0	7.0
11.7	6.5	6.6	4.9	5.1	8.6	8.8	6.5	6.2	7.1	7.3	8.4	8.6	6.6	6.7	7.1	7.0

[a] In Hz, error ± 0.2 Hz. Only $^3J_{HH}$ at the lowest and the highest temperature are tabulated, whereas they are available at several intermediate temperatures in 10 K steps. Note that the complete set of $^3J_{HH}$ between the two extreme temperatures at each pD have been used in the calculation of thermodynamic quantities through pseudorotational analyses and van't Hoff plots. Tabulated coupling constants are the result of simulation and iteration procedure by DAISY program.[16] [b] At 288 K and 358 K.

Table 20. The temperature-dependent vicinal coupling constants in β-D-ddT (**9**) as a function of pD[a]

	β-D-ddT (**9**)															
pD	$^3J_{1'2'}$		$^3J_{1'2''}$		$^3J_{2'3'}$		$^3J_{2'3''}$		$^3J_{2''3'}$		$^3J_{2''3''}$		$^3J_{3'4'}$		$^3J_{3''4'}$	
	278 K	358 K	278 K	358 K	278 K	358 K	278 K	358 K	278 K	358 K	278 K	358 K	278 K	358 K	278 K	358 K
6.8	3.4	4.0	7.2	7.2	8.5	8.7	3.4	4.3	10.3	9.3	8.4	8.6	9.4	8.6	6.2	6.5
7.8	3.4	4.0	7.2	7.2	8.5	8.7	3.4	4.3	10.3	9.3	8.4	8.6	9.4	8.6	6.2	6.5
8.7	3.4	4.1	7.2	7.3	8.5	8.7	3.5	4.3	10.2	9.3	8.4	8.6	9.3	8.6	6.3	6.7
9.2	3.5	4.1	7.2	7.3	8.5	8.7	3.5	4.4	10.2	9.3	8.4	8.5	9.2	8.6	6.2	6.6
9.8	3.6	4.2	7.2	7.1	8.5	8.6	3.6	4.4	10.1	9.3	8.3	8.5	9.1	8.5	6.2	6.5
10.3	3.8	4.4	7.2	7.1	8.6	8.8	3.9	4.5	9.8	9.1	8.5	8.6	9.0	8.4	6.3	6.6
10.9	3.9	4.5	7.2	7.2	8.5	8.7	4.0	4.5	9.6	8.9	8.3	8.5	9.0	8.5	6.3	6.5
11.4	3.9	4.5	7.2	7.2	8.7	8.7	4.0	4.7	9.6	8.8	8.6	8.5	8.9	8.5	6.2	6.6

[a] In Hz, error ± 0.1 Hz for $^3J_{1'2'}$ and $^3J_{1'2''}$, 0.2 Hz for all other $^3J_{HH}$. Only $^3J_{HH}$ at the lowest and the highest temperature are tabulated, whereas they are available at several intermediate temperatures in 10 K steps. Note that the complete set of $^3J_{HH}$ between the two extreme temperatures at each pD have been used in the calculation of thermodynamic quantities through pseudorotational analyses and van't Hoff plots. Tabulated coupling constants are the result of simulation and iteration procedure by DAISY program.[16]

(b) Investigation of the propagation of the error inherent to the experimental $^3J_{HH}$ in terms of the thermodynamics of the two-state N ⇄ S equilibrium. For each set of starting geometries according to (a), we have generated typically 1000 - 3000 sets of $^3J_{HH}$ with a gaussian distribution (σ= 0.1 - 0.2 Hz) around the experimentally measured values. Each of these sets has been used as input for a PSEUROT calculation. The combination of (a) and (b) yielded typically 5000 - 20000 calculations for **1 - 11.**

(c) Van't Hoff type analysis of x_N and x_S calculated by PSEUROT to derive $\Delta H°$, $\Delta S°$ of the N ⇄ S equilibrium. The temperature-dependent x_N and x_S calculated by PSEUROT have been subsequently used in 5000 - 20000 van't Hoff plots to obtain slopes and intercepts, which have been averaged to calculate the average enthalpy ($\Delta H°$) and entropy ($\Delta S°$) values of the N ⇄ S equilibrium in **1 - 11.** The free-energy (ΔG^T) of the N ⇄ S equilibrium at a certain temperature T can be calculated either by adding $\Delta H°$ and $-T\Delta S°$ or directly using the formula: $\Delta G^T = -RT*\ln_{av}(x_S / (1 - x_S))$ from the averaged logarithm of the ratio of x_S and x_N obtained at T with our PSEUROT analyses[2,9]. $\Delta G°$ values reported throughout this paper have been obtained using the second procedure.

Acknowledgements

We thank the Swedish Board for Technical Development, Swedish Natural Science Research (NFR) Council and Swedish Board for Technical Development (NUTEK) for generous financial support. Thanks are due to the Wallenbergstiftelsen, Forskningsrådsnämnden and University of Uppsala for funds for the purchase of 500 MHz and 600 MHz Bruker DRX NMR spectrometers.

References

1. (a) Plavec, J.; Tong, W.; Chattopadhyaya, J. *J. Am. Chem. Soc.* **1993**, *115*, 9734. (b) Plavec, J.; Garg, N.; Chattopadhyaya, J. *J. Chem.Soc., Chem. Commun.* **1993**, 1011. (c) Plavec, J.; Koole, L. H.; Chattopadhyaya, J. *J. Biochem. Biophys. Meth.* **1992**, *25*, 253. (d) Koole. L. H.; Buck, H. M.; Nyilas, A.; Chattopadhyaya, J. *Can J. Chem.* **1987**, *65*, 2089. (e) Koole, L. H.; Buck, H. M.; Bazin, H.; Chattopadhyaya, J. *Tetrahedron* **1987**, *43*, 2289. (f) Koole, L. H.; Plavec, J.; Liu, H.; Vincent, B. R.; Dyson, M. R.; Coe, P. L.; Walker, R. T.; Hardy, G. W.; Rahim, S. G.; Chattopadhyaya J. *J. Am. Chem. Soc.* **1992**, *114*, 9934. (g) Plavec, J.; Thibaudeau, C.; Viswanadham, G.; Sund, C.; Chattopadhyaya, J. *J. Chem. Soc., Chem. Commun.* **1994**, 781. (h) Thibaudeau, C.; Plavec, J.; Watanabe, K. A.; Chattopadhyaya, J. *J. Chem. Soc., Chem. Commun.* **1994**, 537. (i) Thibaudeau, C.; Plavec, J.; Garg, N.; Papchikhin, A.; Chattopadhyaya, J. *J. Am. Chem. Soc.* **1994**, *116*, 4038. (j) Plavec, J.; Thibaudeau, C.; Chattopadhyaya, J. *J. Am. Chem. Soc.* **1994**, *116*, 6558. (k) Thibaudeau, C.; Plavec, J.; Chattopadhyaya, J. *J. Am. Chem. Soc.* **1994**, *116*, 8033. (l) J. Plavec, Ph.D Thesis, Department of Bioorganic Chemistry, Uppsala University, Sweden, **1995**. (m) Plavec, J.; Thibaudeau, C.; Chattopadhyaya, J. *Tetrahedron* **1995**, *51*, 11775. (n) Thibaudeau, C.; Plavec, J.; Chattopadhyaya, J. *J. Org. Chem.* **1996**, *61*, 266. (o) Chattopadhyaya, J. *Nucleic Acids Symposium Series* **1996**, *35*, 111. (p) Plavec, J.; Thibaudeau, C.; Chattopadhyaya, J. *Pure and Applied Chemistry* **1996**, *68*, 2137. (q) Luyten, I.; Thibaudeau, C.; Sandström, A. and Chattopadhyaya, J. *Tetrahedron*, **1997**, *53*, 6433. (r) Luyten, I.; Thibaudeau, C. and Chattopadhyaya, J. *Tetrahedron*, **1997**, *53*, 6903.

2. Our conformational studies are based on the pseudorotational concept[3], which describes the conformation of each sugar pseudorotamer by only two parameters: the phase angle of pseudorotation (P), reflecting which part of the furanose moiety is mostly puckered, and the puckering amplitude (Ψ_m) which shows the extent of the puckering. The hypothesis of a two-state N (North, *C2'-exo-C3'-endo*, $0° < P < 36°$) ⇄ S (South, *C2'-endo-C3'-exo*, $144° < P < 190°$) equilibrium in nucleos(t)ides in solution, originally based on the statistical distribution of X-ray crystal structures[4], has been further corroborated by the NMR observations of the two distinctly identifiable and dynamically interconverting N ⇄ S conformations (as evident by their respective chemical shifts and $^3J_{HH}$) of the constituent sugar moieties in B ⇄ Z DNA[6] or A ⇄ Z RNA[7] or in the A-form ⇄ B-form lariat RNA[8]. The validity of the dynamic two-state N ⇄ S equilibrium in D_2O solution by ^{1}H-NMR is further evidenced by our original observation[1n] that the estimation of its pD-dependent energetics for all β-D-ribo- (β-D-rNs) and β-D-2'-deoxynucleosides (β-D-2'-dNs) in D_2O solution can indeed be used independently to reproduce the literature values[5] of the pK_as of the constituent nucleobases.
3. (a) Kilpatrick, J.E.; Pitzer, K. S. ; Spitzer, R. *J. Am. Chem. Soc.* **1947**, *69*, 2483. (b) Altona, C.; Sundaralingam, M. *J. Am. Chem. Soc.* **1972**, *94*, 8205. (c) Altona, C.; Sundaralingam, M. *J. Am. Chem. Soc.* **1973**, *95*, 2333.
4. de Leeuw, H. P. M; Haasnoot, C. A. G. ; Altona, C. *Isr. J. Chem.* **1980**, *20*, 108.
5. Izatt, R. M.; Christensen, J. J .; Rytting, J. H. *Chem. Rev.* **1971**, *71*, 439.
6. (a) Feigon, J.; Wang, A. H. -J.; van der Marel, G. A.; van Boom, J. H.; Rich, A. *Nucleic Acids Res.* **1984**, *12*, 1243. (b) Tran-Dinh, S.; Taboury, J.; Neumann, J. -M.; Huynh-Dinh, T.; Genissel, B.; Laglois d'Estaintot, B.; Igolen, J. *Biochemistry* **1984**, *23*, 1362.
7. (a) Davis, P. W.; Hall, K.; Cruz, P.; Tinoco, I.; Neilson, T. *Nucleic Acids Res.* **1986**, *14*, 1279. (b) Davis, P. W.; Adamiak, R. W.; Tinoco, I. *Biopolymers* **1990**, *29*, 109.
8. (a) Agback, P.; Sandstrom, A.; Yamakage, S. -I.; Sund, C.; Glemarec, C.; Chattopadhyaya, J. *J. Biochem. Biophys. Methods* **1993**, *27*, 229. (b) Agback, P.; Glemarec, C.; Yin, L.; Sandstrom, A.; Plavec, J.; Sund, C.; Yamakage, S. -I.; Wiswanadham, G.; Rousse, B.; Puri, N.; Chattopadhyaya, J. *Tetrahedron Lett.* **1993**, *34*, 3929.
9. (a) De Leeuw, F. A. A. M. and Altona, C. *J. Comp. Chem.* **1983**, *4*, 428 and PSEUROT, QCPE program No 463. (b) Diez, E.; Fabian, J. S.; Guilleme, J.; Altona, C. and Donders, L. A. *Mol. Phys.* **1989**, *68*, 49. (c) Donders, L. A.; de Leeuw, F. A. A. M. and Altona, C. *Magn. Reson. Chem.* **1989**, *27*, 556. (d) Altona, C.; Ippel, J. H.; Hoekzema, A. J. A. W.; Erkelens, C.; Groesbeek, G.; Donders, L. A. Magn. Reson. Chem. **1989**, *27*, 564. (e) Van Wijk, J., unpublished result. (f) Altona, C.; Francke, R.; de Haan, R.; Ippel, J. H.; Daalmans, G. J.; Westra Hoekzema, A. J. A.; van Wijk, J. *Magn. Res.on Chem.* **1994**, *32*, 670.
10. Edward, J. T. *Chem. Ind. (London)* **1955**, 1102.
11. For review articles on the anomeric effect, see: (a) Tvaroska, I.; Bleha, T. *Adv. Carbohydr.Chem.* **1989**, *47*, 45. (b) Juaristi, E.; Cuevas, G. *Tetrahedron* **1992**, *48*, 5019. (c) Petillo, P. A.; Lerner, L. A. in *The Anomeric Effect and Associated Stereolectronic Effects,* Thatcher, G. R .J. Ed., ACS Symposium Series: Washington, DC, **1993**, pp. 156. (d) Box, V. G. S. *Heterocycles* **1990**, *31*, 1157.
12. (a) Lucken, E. A. C. *J. Chem. Soc.* **1959**, 2954. (b) Romers, C.; Altona, C; Buys, H. R.; Havinga, E. *Top. Stereochem.* **1969**, 4, 39. (c) Perrin, C. L.; Armstrong, K. B.; Fabian, M. A. *J. Am. Chem. Soc.* **1994**, *116*,

715. (d) Salzner, U. *J. Org. Chem.* **1995**, *60*, 986. (e) Cosse-Barbi, A.; Watson, D. G.; Dubois, J. E. *Tetrahedron Lett.* **1989**, *30*, 163.

13. (a) Olson, W. K.; Sussman, J. L. *J. Am. Chem. Soc.* **1982**, *104*, 270. (b) Olson, W. K. *J. Am. Chem. Soc.* **1982**, *104*, 278. (c) Phillips, L.; Wray, V. *J. Chem. Soc., Chem. Commun.* **1973**, 90. (d) Brunck, T.K.; Weinhold, F. *J. Am. Chem. Soc.* **1979**, *101*, 1700. (e) Murcko, M. A.; DiPaola, R. A. *J. Am. Chem. Soc.* **1992**, *114*, 10010. (f) Wiberg, K. B.; Murcko, M. A.; Laidig, K. E.; MacDougall, P. J. *J. Phys. Chem.* **1990**, *94*, 6956.
14. proFit 4.2, Quantum Soft, Postfach 6613, CH - 8023 Zürich, Switzerland, **1990-94**.
15. Wyman, J.; Gill, S. J. *Binding and Linkage. Functional Chemistry of Biological Macromolecules,* University Science Books: Mill Valley, CA **1990**, 330.
16. DAISY, Spin Simulation Program, provided by Bruker, was used with 7 spins systems.
17. (a) Adams, A. D.; Petrie, C. R. and Meyer, R. B. *Nucleic Acids Res.* **1991**, *19*, 3647. (b) Robins, M. J.; Zou, R.; Guo, Z. and Wnuk, S. F. *J. Org. Chem.* **1996**, *61*, 9207.
18. Vorbruggen, H. *Chem. Ber.* **1981**, *114*, 1234.
19. Davoll, J. and Lowy, B. A. *J. Am. Chem. Soc.* **1951**, *73*, 1650.
20. (a) Augestad, I. and Berner, E. *Acta Chem. Scand.* **1954**, *8*, 251. (b) Földesi, A.; Nilsson, F. P. R.; Glemarec, C.; Gioeli, C. and Chattopadhyaya, J. *Tetrahedron* **1992**, *48*, 9033.
21. Robins, M. J.; Wilson, J. S. and Hansske, F. J. *J. Am. Chem. Soc.* **1983**, *105*, 4059.
22. Janardhanam, S. and Nambiar, K. P. *J. Chem. Soc., Chem. Commun.* **1994**, 1009.
23. Okabe, M.; Sun, R.-C.; Tam, S. Y.-K.; Todaro, L. J. and Coffen, D. L. *J. Org. Chem.* **1988**, *53*, 4780.
24. (a) Saffhill, R. and Reese, C. B. *J. C. S. Perkin I* **1972**, 2937. (b) Kamimura, T.; Tsuchiya, M.; Urakami, K-i.; Koura, K.; Sekine, M.; Shinozaki, K.; Miura, K-i. and Hata, T. *J. Am. Chem. Soc.* **1984**, *106*, 4552.
25. Yano, J.; Kan, L. S. and Ts'o, P. O. P. *Biochim. Biophys. Acta* **1980**, *629*, 178.
26. Rosemeyer, H.; Tóth, G.; Golankiewicz, B.; Kazimierczuk, Z.; Bourgeois, W.; Kretschmer, U.; Muth, H.-P. and Seela, F. *J. Org. Chem.* **1990**, *55*, 5784.

(*Received in UK* 12 *June* 1997; *revised* 5 *August* 1997; *accepted* 7 *August* 1997)